



Solubility of high-magnesium calcite in seawater and its implementation in (Py)CO2SYS

Ben A. Cala^{1,2}, Mariette Wolthers², Olivier Sulpis³, Jonathan D. Sharp^{4,5}, and Matthew P. Humphreys¹

¹NIOZ Royal Netherlands Institute for Sea Research, Department of Ocean Systems (OCS), Texel, The Netherlands

²Utrecht University, Department of Earth Sciences, Princetonlaan 8A, 3584 CB Utrecht, The Netherlands

³CEREGE, Aix Marseille Univ, CNRS, IRD, INRAE, Aix-en-Provence, France

⁴Cooperative Institute for Climate, Ocean, and Ecosystem Studies, University of Washington, Seattle, WA, USA

⁵Pacific Marine Environmental Laboratory, National Oceanic and Atmospheric Administration, Seattle, WA, USA

Correspondence: Ben A. Cala (ben.cala@nioz.nl)

Abstract.

The calcium carbonate pump is an important part of the ocean's carbon cycle but our knowledge of it is incomplete. For example, alkalinity data suggest that carbonate mineral dissolution happens at shallow depths where bulk seawater is oversaturated with respect to calcite and aragonite. It has been hypothesised that high-Mg calcites could explain this discrepancy due

5 to their high solubility. However, our knowledge of what depth Mg calcites start dissolving and how they might respond to continuing ocean acidification is limited because their solubility in marine environments is poorly known. Here, we develop an approach to calculate Mg calcite solubility by using published solubility data under standard laboratory conditions and adding dependencies for temperature, salinity and pressure for ranges relevant to the marine environment. We then implement this

10 into the CO2SYS software family (Python and GNU Octave/Matlab versions) and calculate saturation states globally for Mg calcites with different Mg%. Our results reveal that, contrary to previous assumptions, the saturation horizon for many high-Mg calcites often lies deeper than that of aragonite, suggesting that high-Mg calcites are unlikely to account for shallow-water carbonate dissolution. Our model aligns with the few existing in situ particle dissolution measurements of Mg calcites, but many unknowns remain regarding the solubility of Mg calcites in marine environments and future experiments focusing on temperature and pressure dependence are needed to better constrain their role in the marine carbon cycle.

15 1 Introduction

Carbonate minerals are an important part of the marine carbon cycle. Many organisms, such as coccolithophores, foraminifera, pteropods, and corals, build their shells or skeletons out of calcium carbonate (CaCO_3), mainly in the form of calcite and aragonite (e.g., Sarmiento and Gruber, 2013). The dissolution of these shells increases seawater alkalinity, which acts as a buffer and enhances the capability of the ocean to take up more CO_2 without significantly affecting pH:





Whether calcite or aragonite dissolve is governed by the saturation state Ω . For calcite, this is given by

$$\Omega_C = \frac{[\text{Ca}^{2+}][\text{CO}_3^{2-}]}{K_C^*(T, S, p)} \quad (1)$$

where $K_C^*(T, S, p) = ([\text{Ca}^{2+}][\text{CO}_3^{2-}])_{\text{sat}}$ is the equilibrium constant (also called the solubility product) of calcite.

The process of carbonate production and dissolution is termed the carbonate counter pump, one of several pumps in the ocean that distribute carbon in the water column. The carbonate pump is poorly constrained: there are large uncertainties about the contributions of the different carbonate minerals, how much is produced where, how much is exported in what form, and how quickly and where in the water column or the sediment the minerals dissolve (Berelson et al., 2007; Liang et al., 2023; Kwon et al., 2024). The last point is especially relevant when considering the buffering effect of alkalinity, as shallow-water dissolution may return alkalinity to the surface on short time scales through mixing, whereas dissolution deep in the water column can sequester alkalinity for thousands of years.

Water column analysis of alkalinity profiles reveal that most dissolution happens in the upper 1000 m where bulk seawater is often still oversaturated ($\Omega > 1$) with respect to calcite and to aragonite (Sulpis et al., 2021). Proposed explanations include dissolution in zooplankton guts or metabolically mediated dissolution where micro-environments could lead to local undersaturation (Milliman et al., 1999; White et al., 2018; Subhas et al., 2022; Dong et al., 2025). However, another hypothesis is that a more soluble form of carbonate mineral, magnesium (Mg) calcite, where Ca^{2+} ions are randomly replaced by smaller Mg^{2+} ions, may also contribute to shallow dissolution (Morse and Mackenzie, 1990; Morse et al., 2006; Wilson et al., 2009). This remains difficult to evaluate because no simple method exists to calculate in situ saturation state of Mg calcites.

Mg calcites are produced by a variety of marine organisms as part of their skeletal structures, most commonly red coralline algae (8 to 29 Mg%), benthic foraminifera (0 to 16 Mg%), bryozoans (0 to 11 Mg%), echinoderms (5 to 16 Mg%) and barnacles (1 to 5 Mg%), but other organisms contribute as well, such as calcareous sponges, brachiopods, molluscs, annelid worms and some stony corals (Chave, 1954; Morse and Mackenzie, 1990). How much Mg is incorporated is controlled mainly by temperature but also depends on light, nutrient concentrations and Ω (Chave, 1954; Moberly, 1968; Agegan, 1985), leading Mg content to decrease with increasing latitude and water depth. Mg content in modern tropical or subtropical shoal and shelf calcareous sediment is approximately 14% (Garrels and Wollast, 1978; Agegan and Mackenzie, 1989). Mg calcites with ~12 Mg% are formed abiotically as marine cements in shallow, warm waters (Garrels and Wollast, 1978; Mucci, 1987). Teleost fish have been recognised as significant producers of high Mg calcite as part of their osmoregulatory strategy (Walsh et al., 1991; Wilson et al., 2009; Grosell, 2011); recent estimates of their contribution to CaCO_3 production could match those of foraminifera and coccolithophores (Oehlert et al., 2024a). The fish-produced Mg calcite (also called ichthyocarbonate) is highly heterogeneous in morphology, size, and mineralogy and exhibits a wide range of Mg contents (0.5 to > 40 Mg%), both within and between species (Perry et al., 2011; Salter et al., 2012; Folkerts et al., 2024).

Anthropogenic CO_2 emissions continue to rise, a quarter of which are absorbed by the ocean (Friedlingstein et al., 2025). This helps mitigate climate change, but the rising partial pressure of CO_2 ($p\text{CO}_2$) in seawater lowers seawater pH, a process referred to as ocean acidification. Because Mg calcite producers are abundant in shallow and warm waters, they may be the first to be affected by ocean acidification, decreasing calcification rates and making it impossible for the organisms to maintain



55 their shells (Orr et al., 2005; Andersson et al., 2008). At the same time, dissolution of the most soluble Mg calcite phases might provide a local buffer against a further decrease in pH and thus protect less soluble phases until all of the highest soluble phase is dissolved (Morse et al., 2006). To explore these processes further, a good knowledge is needed of the saturation states that these high Mg calcites experience and how those saturation states may change with ocean acidification and rising seawater temperatures.

60 1.1 Challenges of estimating Mg calcite solubility

There are several reasons why the solubility of Mg calcite is more complicated to measure, understand and implement in models than it is for calcite and aragonite.

1.1.1 Quantification of solubility

When the solubility for calcite or aragonite is measured, equilibrium can be approached and reached from both under- and 65 oversaturation (Mucci, 1983). This is not possible for Mg calcites. For one, equilibrium is not reached during the dissolution of Mg calcite because at some point during the dissolution process, less soluble phases such as low Mg calcite or calcite starts to precipitate. Only during the first stage of dissolution, so-called congruent dissolution, does Mg calcite react with a fixed composition and the ratio of $[Mg^{2+}]$ to $[Ca^{2+}]$ in the solution stays constant (see Plummer and Mackenzie (1974) and Morse and Mackenzie (1990) for more detailed discussions of the different dissolution stages). During this congruent stage, 70 Mg calcite can be treated as a single component phase instead of the two-component solid that it is. Thorstenson and Plummer (1977) introduced the concept of “stoichiometric saturation” which differs from “thermodynamic saturation” in that it captures the dissolution of the mixed phases in the solid solution series. At stoichiometric saturation, the equilibrium constant (K_{MC}) can be expressed as the ion activity product (IAP):

$$K_{MC} = IAP = a(Mg^{2+})^x a(Ca^{2+})^{1-x} a(CO_3^{2-}) \quad (2)$$

75 where a_i is the activity of the ion (the ‘effective concentration’ that arises due to interactions of the solutes and solvent), and x is the mole fraction of $MgCO_3$ in calcite. Other expressions for the equilibrium constant (e.g. $a(Ca^{2+}) \cdot a(CO_3^{2-})$ and $(a(Mg^{2+}) + a(Ca^{2+})) \cdot a(CO_3^{2-})$) have been proposed but are not discussed further here, since Walter and Morse (1984) showed that they yield different equilibrium constants when the composition of the solution is changed and are thus not valid.

In many past investigations of Mg calcite solubility, pH measured during the congruent stage of dissolution was plotted 80 against the inverse of the square root of time and the linear portion extrapolated to infinite time (i.e., $time^{-0.5} = 0$) to find the equilibrium pH, circumventing the problem of calcite precipitation. There is no theoretical basis as to why $time^{-0.5}$ is used for the extrapolation to infinite time. Rather, it was chosen because it yielded linear plots as infinite time and the equilibrium pH were approached. This works better for slow reactions and it does not work if there is a change in the dissolution mechanism, which is why experiments were usually conducted at low undersaturation (Plummer and Mackenzie, 1974). From the equilibrium pH and the solution composition, the activities of CO_3^{2-} , Mg^{2+} and Ca^{2+} are inferred and the equilibrium constant calculated with Eq.(2). Whether this kinetic approach to determine the solubilities of Mg calcites is indeed valid has been



debated extensively in the literature (Morse and Mackenzie, 1990). Lafon (1978) showed that extrapolation to infinite time against time^{-0.5} generally leads to incorrect estimates of the equilibrium value and that there is no reason why it should work for Mg calcite. Nevertheless, it is the most widely used method (e.g. Chave et al. (1962); Plummer and Mackenzie (1974); Bischoff et al. (1987); Walter and Morse (1984); Bertram et al. (1991); Woosley et al. (2012)).

Another method to avoid precipitation was employed by Busenberg and Plummer (1989) who added KH₂PO₄ to the solution which delayed the onset of incongruent dissolution by inhibiting nucleation of more stable lower Mg calcite. When the same IAP was maintained for several days, they assumed that IAP = K_{MC}. Mucci and Morse (1984) used a third method, only applicable to synthetic Mg calcites, which are precipitated on calcite from aqueous solutions with different Mg to Ca ratios. This is the only method that does not rely on the concept of stoichiometric equilibrium and approaches equilibrium from oversaturation. Encouragingly, there is good agreement between the measured synthetic Mg calcite solubilities for all three methods (Busenberg and Plummer, 1989), suggesting that the data of all three methods can be used alongside each other.

1.1.2 Consequences of sample types and treatments

In contrast to calcite and aragonite, for which thermodynamic equilibrium can actually be reached, measurements for Mg calcite solubility, often relying on a kinetic approach, are more affected by the sample type and preparation as these influence the kinetic behaviour of the sample and therefore the extrapolation to infinite time (e.g. the (non-)existence of an inflection point (Plummer and Mackenzie, 1974; Lafon, 1978)).

The highest solubility was measured in biogenic samples that were minimally treated before the experiments (Plummer and Mackenzie, 1974). At 12 Mg% ($x = 0.12$), they measured a solubility that was 2.5 to 3 times higher than other measurements (Walter and Morse, 1984; Bischoff et al., 1987). Those later measurements used biogenic samples that were ultrasonically cleaned, bleached to eliminate organic matter, and annealed. This led to a decrease in reactive surface area stemming from submicron-sized particles and crystal strain introduced by sample crushing. More rapid dissolution rates can potentially lead to erroneous extrapolations of the equilibrium pH (see previous section) and consequently an overestimation of solubility.

Not only is the preparation of the sample important but also the type of sample itself, (i.e. whether they are of inorganic or biogenic origin), which affects the microstructure of the mineral. Mackenzie et al. (1983) called biogenic Mg calcites “sloppy” in comparison to well-crystallised and homogeneous synthetic phases. Busenberg and Plummer (1989) showed that the solubility is significantly increased if there are structural defects present. Biogenic samples for instance include substitutions by other ions such as Na⁺ and/or SO₄²⁻, and dislocations in the crystal lattice.

Ultimately, three different categories emerged in which all the solubility measurements were sorted (Fig.1). Category 1 (which we term “fresh”) is solely the data from the minimally prepared/untreated samples by Plummer and Mackenzie (1974). Category 2 (“with defects”) includes minerals with structural defects. This covers biogenic samples that are not in category 1 because they underwent some treatment prior to measurement (e.g. cleaned to remove organics and/or annealed to get rid of very reactive surface areas), as well as synthetic samples that are massively defective (i.e. many in the experiment by Busenberg and Plummer (1989) because they were, for example, prepared at high calcite supersaturations from NaCl–Na₂SO₄–MgCl₂–CaCl₂ solutions). Category 3 (“no defects”) encompasses all the remaining synthetic phases and



also natural inorganic samples of metamorphic and hydrothermal origin that consist of a single Mg calcite phase and no other components. For the most part, except at very low Mg content, minerals in category 1 are the most unstable and in the third the most stable. It is possible that over long time frames Mg calcites stabilise through diagenetic alterations (e.g., through changes in the relative amounts of trace element contaminants, or cation ordering) and consequently change categories (Bischoff et al., 125 1993). The question as to which category is “best” or “most correct” cannot be answered generally but must be evaluated based on the context. Category 1 might be the best approximation of the reactivity of “fresh” biogenic Mg calcite in the water column (Morse et al., 2006), whereas the solubility of samples from the sediment might be better described by categories 2 or 3.

1.1.3 Lack of comprehensive datasets across conditions

When Mucci (1983) parameterised calcite and aragonite solubility for temperature and salinity, he performed nearly 480 130 independent measurements. Many more would be needed to accomplish the same for Mg calcites because of the additional degree of freedom: the amount of Mg present in the mineral. The same is true for pressure. Considering the high number of measurements needed and the difficulties described earlier to make these measurements, it is not surprising that not many studies have attempted this task. Only one study exists (Bertram et al., 1991) that measured the solubility of several synthetic Mg calcites at different temperatures, but not with the overall goal to parameterise temperature dependence and Mg content. 135 Further, it is unknown whether their findings can be applied to biogenic samples.

1.2 Aims of this study

In this work, we parameterise Mg calcite solubility based on past dissolution measurements so it can be integrated in marine 140 carbonate system solving software and be used in marine contexts. We convert the measured thermodynamic equilibrium constants (expressed as activities) to stoichiometric equilibrium constants (expressed as concentrations). We add temperature and pressure dependence by applying what is known for calcite and magnesite to Mg calcite under the simplifying assumption 145 of an ideal solid solution. We implement these calculations in the CO2SYS family of software (for PyCO2SYS for Python and MATLAB/GNU Octave), which is a well established and widely used tool in the research field to solve the carbonate system and calculate other properties of interest, such as carbonate mineral saturation states. Although Mg calcite solubility has been studied extensively in the last seven decades, many gaps in the research still remain or experimental results have not been consistent and this parameterisation aims to reflect our uncertainty by providing several options for how, for instance, 150 temperature dependence is calculated. In the second half of the paper, we apply the implementation to a global dataset to investigate the spatial distributions of Mg calcite saturation states.

2 Methods

Solubility data for Mg calcites is usually available only as a thermodynamic equilibrium constant K (expressed in activities 150 and also called the solubility product K_{sp}) measured at 25 °C and 1 atm.



Table 1. Measurements for the solubility of different Mg calcites at 25 °C and 1 atm used in this study. The different categories are explained in Sect. 1.1.2.

Category	Description	Source	Data points	Sample origin
1	Fresh	Plummer and Mackenzie (1974), recalculated by Thorstenson and Plummer (1977)	10	Biogenic
		Bischoff et al. (1987)	9	Biogenic
	With defects	Walter and Morse (1984)	1†	Biogenic
2	With defects	Busenberg and Plummer (1989)	11	Biogenic
		Busenberg and Plummer (1989)	8	Synthetic, NaCl + K ₂ SO ₄ solution
		Busenberg and Plummer (1989)	7	Synthetic, NaCl solution
3	No defects	Bischoff et al. (1987)	9	Synthetic
		Mucci and Morse (1984)	6	Synthetic
	No defects	Busenberg and Plummer (1989)	28	Natural inorganic

† The other data point in the paper is excluded because the sample also included brucite (MgOH₂).

However, to be able to calculate the saturation state of Mg calcites in conditions present of the marine environment, the stoichiometric equilibrium constant K^* is needed, which is expressed as a function of Mg content (x), temperature (T), salinity (S) and pressure (p). This is achieved in four steps:

$$\xrightarrow{1} K(x) \xrightarrow{2} K(x, T) \xrightarrow{3} K^*(x, T, S) \xrightarrow{4} K^*(x, T, S, p)$$

155 2.1 Step 1: Solubility data categorisation and K fits

The sources for all solubility measurements along with the number of data points and sample types are given in Table 1. Measurements are sorted into the categories that have historically been used (Sect. 1.1.2). Only measurements that ensured that no incongruent dissolution took place during the experiment are included.

We fitted a third degree polynomial to the measurements (Table 1) in each category (Fig. 1), resulting in the following 160 equations:

Category 1 (fresh biogenic):

$$\log_{10} K_1 = -234.13194855x^3 + 85.74778794x^2 - 1.61786329x - 8.51219119 \quad (3)$$

Category 2 (with defects):

$$\log_{10} K_2 = -20.12671951x^3 + 14.0201507111x^2 - 1.27685236x - 8.29393478 \quad (4)$$

165 Category 3 (no defects):

$$\log_{10} K_3 = -10.47008999x^3 + 8.41626295x^2 - 0.10607321x - 8.50230163 \quad (5)$$

Covariance matrices for these fits are given in the SI.

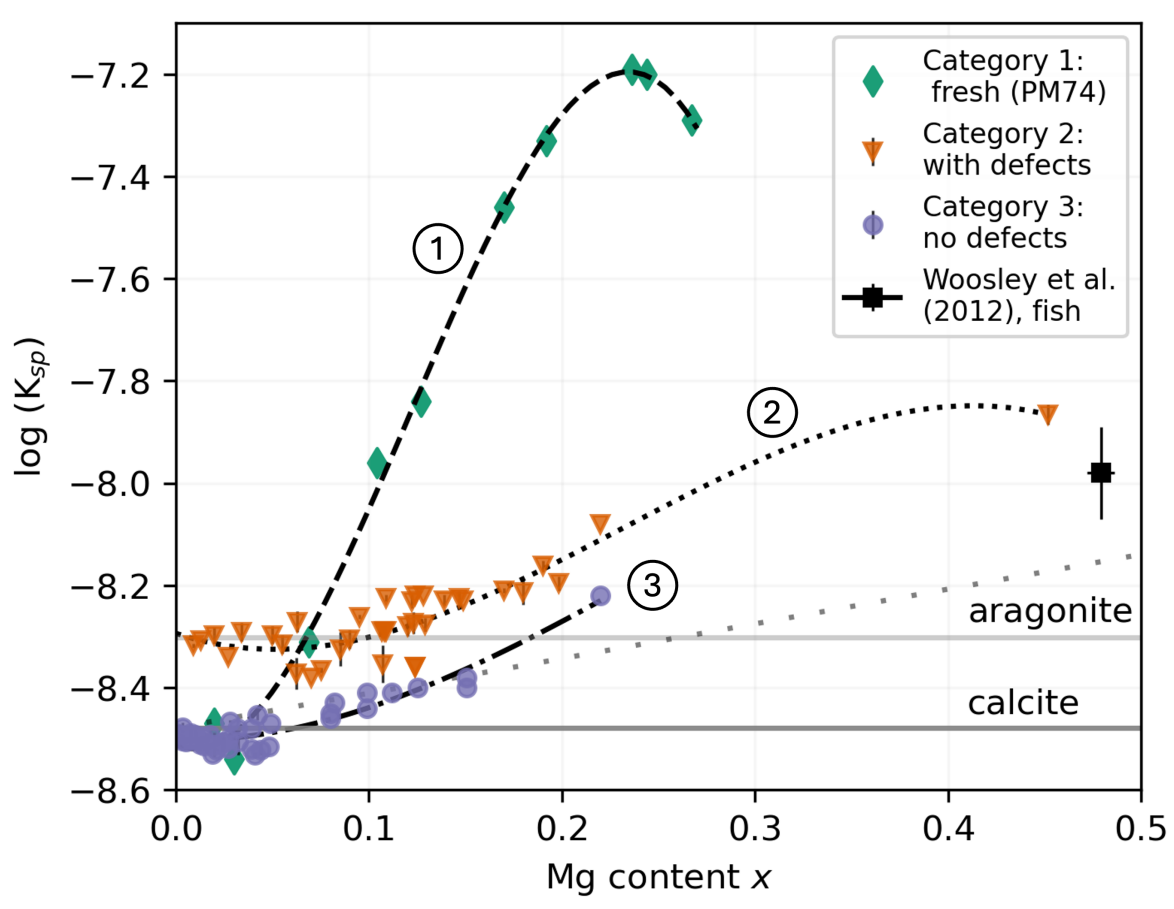


Figure 1. Best fits of $\log_{10} K_{sp}$ (equations 3 to 5) for the three solubility categories (Sect. 1.1.2) for Mg calcites at 25 °C and 1 atm, plotted against Mg content x . Sources for the data points are given in Table 1. The calcite and aragonite solubility are shown as grey horizontal lines for comparison and the loosely dotted line represents the ideal solid solution line between calcite and magnesite.

2.2 Step 2: Temperature dependence

Like all equilibrium constants, K is temperature dependent. One study has investigated the temperature dependence of Mg calcites (Bertram et al., 1991) but only at temperatures between 25 and 64 °C which does not represent marine environments. That study concluded that the temperature dependence of Mg calcites is comparable to that of calcite and aragonite between 25 and 45 °C. Assuming that this trend continues below 25 °C, one option to account for the temperature dependence is offsetting the equilibrium constant of calcite. Another option stems from the description of Mg calcites as solid solutions between the calcite and magnesite ($MgCO_3$) endmembers. A third option is to use the van't Hoff equation, which quantifies the theoretical temperature-sensitivity of equilibrium constants. These three options are described below in increasing order of complexity.



2.2.1 Calcite-like

Plummer and Busenberg (1982) found the temperature dependence of K_C to be

$$\log_{10} K_C = -171.9065 - 0.077993 \cdot T + \frac{2839.319}{T} + 71.595 \log_{10} T \quad (6)$$

To adjust for the different solubility of Mg calcites compared to calcite, the difference in their solubility is determined at 180 25 °C:

$$\Delta \log_{10} K(25^\circ\text{C}) = \log_{10} K_C(25^\circ\text{C}) - \log_{10} K_{MC}(25^\circ\text{C}) \quad (7)$$

$K_{MC, \text{ca-like}}(T)$ is then obtained by

$$\log_{10} K_{MC, \text{ca-like}}(T) = \log_{10} K_C(T) - \Delta \log_{10} K(25^\circ\text{C}) \quad (8)$$

2.2.2 Ideal solid solution

185 If Mg calcite were an ideal solid solution calcite and magnesite, then

$$\log_{10} K_{MC, \text{ideal, general}} = (1-x) \log_{10} K_C + x \log_{10} K_M \quad (9)$$

This is not the case; the measured $\log_{10} K$ are usually higher (Fig. 1). This may be due to differences in cation ordering in the solid phases and/or non-linear influence of Mg incorporation on the solubility of Mg calcites (Koskamp et al., 2021).

However, ideal solid solutions could still provide a useful framework for temperature dependence. Bénédith et al. (2011) 190 measured the temperature dependence of magnesite between 50 and 200 °C (according to that study, measurements below 50 °C are “extremely difficult to perform”). They found that the solubility product of magnesite has a stronger dependence on temperature than calcite does:

$$\log_{10} K_M = 7.267 - 0.033918 \cdot T - \frac{1476.604}{T} \quad (10)$$

which at 25 °C results in $\log_{10} K_M = -7.80$. A combination of the calcite and magnesite temperature dependence would 195 therefore lead to a steeper curve than solely using the calcite temperature dependence as done in the previous section. The implementation in PyCO2Sys is similar to Eq. (7) and (8): To adjust for the non-ideal behaviour of Mg calcite, the difference in the solubility between the ideal (Eq. (9) with Eq. (6) and (10)) and the measured (equations 3 to 5) K_{MC} is determined at 25 °C:

$$\Delta \log_{10} K(25^\circ\text{C}) = \log_{10} K_{MC, \text{ideal, general}}(25^\circ\text{C}) - \log_{10} K_{MC}(25^\circ\text{C}) \quad (11)$$

200 $K_{MC, \text{ideal}}(T)$ is then obtained by

$$\log_{10} K_{MC, \text{ideal}}(T) = \log_{10} K_{MC, \text{ideal}}(T) - \Delta \log_{10} K(25^\circ\text{C}) \quad (12)$$



2.2.3 Van't Hoff equation

For a constant reaction entropy, the van't Hoff equation is

$$\frac{d\ln(K)}{dT} = \frac{\Delta H_r(T)}{RT^2} \quad (13)$$

205 with R as the gas constant and ΔH_r as the reaction enthalpy, which can be calculated from Hess's law:

$$\Delta H_r^\circ = \sum \Delta H_f^\circ(\text{products}) - \sum \Delta H_f^\circ(\text{reactants}) \quad (14)$$

For calcite, at standard conditions, this is

$$\Delta H_r^\circ = \Delta H_f^\circ(\text{CaCO}_3) - (\Delta H_f^\circ(\text{Ca}^{2+}) + \Delta H_f^\circ(\text{CO}_3^{2-})) \quad (15)$$

The variance of ΔH with temperature is given by Kirchhoff's Law of Thermochemistry, which states that

210 $\Delta(\Delta H) = C_p \cdot \Delta T \quad (16)$

where C_p is the heat capacity at constant pressure.

Heat capacities for individual ions (e.g., CO_3^{2-}) are generally not available as they cannot be directly measured due to solvation effects and the lack of a reference state. Therefore, only the solid phase (e.g., CaCO_3) is considered in the heat capacity term. It follows that

215 $\Delta H_r(T) = \Delta H_r(T_0) + C_p(\text{CaCO}_3) \cdot (T - T_0) \quad (17)$

Here, T_0 is the reference temperature of 25 °C for which we know ΔH and K . Substituting Eq. (17) into (13) results in

$$\int_{T_0}^T d\ln K = \int_{T_0}^T \frac{\Delta H_r(T_0) + \Delta C_p(T - T_0)}{RT^2} dT \quad (18)$$

$$= \frac{\Delta H_r(T_0)}{R} \int_{T_0}^T \frac{1}{T^2} dT + \frac{C_p}{R} \int_{T_0}^T \frac{1}{T} - \frac{T_0}{T^2} dT \quad (19)$$

Integration yields this final expression to calculate K at varying temperatures:

220 $K_{\text{vH}}(T) = K(T_0) \cdot \exp \left[-\frac{\Delta H_r}{R} \left(\frac{1}{T} - \frac{1}{T_0} \right) - \frac{C_p}{R} \left(\ln \left(\frac{T}{T_0} \right) + \frac{T_0}{T} - 1 \right) \right] \quad (20)$

Both ΔH_r and C_p are dependent on the Mg content of Mg calcites. As in the previous section, we calculate them by assuming an ideal solid solution between calcite and magnesite for Mg calcites. Bischoff (1998) found that biogenic calcites generally fall above this ideal mixing line for the dissolution enthalpy while synthetic Mg calcites fall below it (Fig. 1, ibid.). For our purposes, the ideal line in the middle might therefore be an acceptable choice. Thus, $\Delta H_r^\circ(x)$ can be modelled by

225 $\Delta H_{r,\text{MC}}^\circ(x) = (1 - x)\Delta H_{r,C}^\circ + x\Delta H_{r,M}^\circ \quad (21)$



where



230 calculated from the enthalpies of formation of Robie and Hemingway (1995).

The ideal solid solution assumption is transferred to C_p :

$$C_{p,\text{MC}}(x) = (1-x)C_{p,\text{C}} + xC_{p,\text{M}} \quad (\text{22})$$

where $C_{p,\text{C}} = 81.88 \text{ J mol}^{-1} \text{ K}^{-1}$ and $C_{p,\text{M}} = 75.52 \text{ J mol}^{-1} \text{ K}^{-1}$ (Reed, 2020).

For this approach we assume that the reaction entropy is constant across temperatures. According to Bischoff (1998), the variability in the entropic contribution to Mg calcite dissolution is very limited, ranging from $-2 \text{ J mol}^{-1} \text{ K}^{-1}$ for 2 Mg% to $-5 \text{ J mol}^{-1} \text{ K}^{-1}$ for 15 Mg% at 25 °C.

2.3 Step 3: Conversion to stoichiometric equilibrium constant

In most marine contexts, only the concentrations c_i of the ions are known and not the activities a_i . Therefore, to calculate the saturation state, the stoichiometric solubility product K^* is needed. Activities can be converted to concentrations with the 240 activity coefficient γ_i :

$$[c]_i = \frac{a_i}{\gamma_i} \quad (\text{23})$$

Thus, the stoichiometric solubility product for Mg calcites can be calculated via

$$K_{\text{MC}}^*(x, T, S) = \frac{K_{\text{MC}}(x, T)}{\gamma_{\text{Mg}}^x \cdot \gamma_{\text{Ca}}^{1-x} \cdot \gamma_{\text{CO}_3}} \quad (\text{24})$$

Note that the mole fraction of MgCO_3 is taken into account, same as in Eq. (2) for the IAP.

245 Activity coefficients were calculated with Pytzer (version 0.6.0) (Humphreys and Schiller, 2024), a Python implementation of the Pitzer model, using the CWTD23 library (Clegg et al., 2023) (this gives comparable/the same results as the MarChem-Spec software). The activity coefficients directly obtained from Pytzer cannot be used in Eq. (24), as they need to be adjusted for the ion pairs that are explicitly modelled in Pytzer but not in (Py)CO2SYS. Consequently, total activity coefficients γ_i^t (Fig. S1) are calculated by

$$250 \quad \gamma_{\text{Mg}^{2+}}^t = \frac{\gamma_{\text{Mg}^{2+}} \cdot m_{\text{Mg}^{2+}}}{m_{\text{Mg}^{2+}} + m_{\text{MgCO}_3^\circ} + m_{\text{MgF}^+} + m_{\text{MgOH}^+}} \quad (\text{25})$$

$$\gamma_{\text{Ca}^{2+}}^t = \frac{\gamma_{\text{Ca}^{2+}} \cdot m_{\text{Ca}^{2+}}}{m_{\text{Ca}^{2+}} + m_{\text{CaCO}_3^\circ} + m_{\text{CaF}^+}} \quad (\text{26})$$



$$\gamma_{\text{CO}_3^{2-}}^t = \frac{\gamma_{\text{CO}_3^{2-}} \cdot m_{\text{CO}_3^{2-}}}{m_{\text{CO}_3^{2-}} + m_{\text{CaCO}_3} + m_{\text{MgCO}_3} + m_{\text{SrCO}_3}} \quad (27)$$

255 where m_i is the molality of species i .

Here, γ_i is a function of only salinity and temperature, since the ratio of different ions in seawater (Millero et al., 2008) can be assumed constant as the activity coefficients change less than 1% by varying dissolved inorganic carbon (DIC) and total alkalinity (TA) (Fig. S2 and S3). We parameterised the three activity coefficients γ_i^t for the most relevant ranges of temperature (270 to 320 K) and salinity (5 to 45). By inspection, we found that the temperature dependence of γ_i^t can be represented by an
 260 equation of the form:

$$\gamma_i^t(T) = a - c \cdot (T - b)^{\frac{1}{d}} \cdot \ln((T - b) \cdot e) \quad (28)$$

Each parameter a, b, c, d, e was fitted to include the dependence on salinity of γ_i^t , represented by

$$\gamma_i^t(S) = a_0 + a_1 \cdot \left(\frac{1}{S + a_2} \right) \quad (29)$$

This results in 15 total parameters that describe each γ_i^t (Table 2). The parameters were fitted using SciPy's (Virtanen et al.,
 265 2020) *curve_fit* function. The root mean squared error (RMSE) was < 0.0002 for all activity coefficients. $\gamma_{\text{Mg}^{2+}}^t$ is captured best (Fig. S4a); the highest deviation of the parameterised activity coefficients are at the extremes of the temperature and low end of salinity range for the carbonate ions but they are still off by less than 1% of the calculated values (Fig. S4c). With this parameterisation, the activity coefficients at standard conditions (25 °C, 35 salinity, 1 atm) are

$$\gamma_{\text{Mg}^{2+}} = 0.2034 \quad \gamma_{\text{Ca}^{2+}} = 0.1886 \quad \gamma_{\text{CO}_3^{2-}} = 0.0432$$

270 Using these values for γ and Eq. (6) and (24) to calculate the equilibrium constant of calcite results in -6.39 which is in good agreement with $K_{\text{C}}^* = -6.37$ from Mucci (1983).

2.4 Step 4: Pressure dependence

The variation of K^* with pressure is also temperature dependent and is described by Millero (1979) as

$$\ln \frac{K_p^*}{K_0^*} = -\frac{\Delta V}{RT} p + 0.5 \frac{\Delta K}{RT} p^2 \quad (30)$$

275 where p is pressure and ΔV denotes volume and ΔK compressibility changes. For calcite, ΔV and ΔK are calculated following Ingle (1975):

$$\Delta V_{\text{C}} = -48.76 + 0.5304 \cdot \Theta \quad (31)$$

$$\Delta K_{\text{C}} = (-11.76 + 0.3692 \cdot \Theta) \cdot 10^{-3} \quad (32)$$



Table 2. Parameters to represent the activity coefficients γ_i^t of the ions Mg^{2+} , Ca^{2+} and CO_3^{2-} with equations (28) and (29).

	Mg^{2+}	Ca^{2+}	CO_3^{2-}
a_0	-8.995205	0.077695	-0.015668
a_1	29429.845	2.281375	77.140941
a_2	3413.656	10.898043	7.768101
b_0	446.73519	269.207962	-5073.189
b_1	41058.158	-58.252	-951872680
b_2	-161.85	0.127866	1368302773
c_0	0.047231	0.007541	0.000000
c_1	0.146212	0.084482	0.191966
c_2	4.462621	2.274432	6.415768
d_0	-51.495749	0.467107	1.370889
d_1	331316	370.905	-1628.535
d_2	6100.392	150.378	-5205.24
e_0	0.001091	0.007527	0.002003
e_1	-0.000199	-0.025242	-0.005675
e_2	-0.811412	3.080641	7.988860

280 with temperature Θ in degrees Celsius.

Since ΔK is assumed equal for calcite and aragonite, the same is adopted for Mg calcites:

$$\Delta K_{MC} = \Delta K_C \quad (33)$$

285 ΔV depends on the molar volume V_m (but $\Delta V \neq V_m$). For aragonite, V_m is $2.8 \text{ cm}^3 \text{ mol}^{-1}$ lower than for calcite, therefore the change in ΔV is also less: $\Delta V_A = \Delta V_C + 2.8$ (ΔV is negative). For Mg calcites, V_m depends on the Mg content. As before, we assume that V_m behaves like it would for an ideal solid solution between calcite and magnesite:

$$\Delta V_{MC} = \Delta V_C + (V_{m,C} - V_{m,M}) x \quad (34)$$

The molar volume V_m is calculated with

$$V_m = \frac{N_A \cdot V_{cell}}{Z}, \quad (35)$$

where N_A is the Avogadro constant and Z is the number of formula units in the unit cell, here $Z = 6$. Cell volumes V_{cell} for calcite and magnesite are taken from Robie and Bethke (1962). Comparison to measurements of Mg calcite V_{cell} (Bischoff, 1985; Paquette and Reeder, 1990; Althoff, 1977) show that the ideal mixing line is slightly overestimating V_m but is a reasonable approximation ($R^2 = 0.93$, Fig. S5). ΔV_{MC} is thus implemented as $\Delta V_{MC} = \Delta V_C + 8.9x$ which at 15 Mg% and 25 °C results in $\Delta V_{MC} = -36.84$.



2.5 Implementation in PyCO2SYS

295 The saturation state Ω with respect to Mg calcites is calculated with

$$\Omega_{\text{MC}}(x, T, S, p) = \frac{[\text{Mg}^{2+}]^x [\text{Ca}^{2+}]^{1-x} [\text{CO}_3^{2-}]}{K^*(x, T, S, p)} \quad (36)$$

In (Py)CO2SYS, $[\text{Ca}^{2+}]$ (Riley and Tongudai, 1967) and $[\text{Mg}^{2+}]$ (Millero et al., 2008) are both calculated from salinity. $[\text{CO}_3^{2-}]$ can either be directly input or calculated from two other carbonate system parameters. The user can input for which (range of) Mg content x K^* and Ω should be calculated. If x is outside of the range for which K has been fit (Fig. 1), a warning 300 is given but the calculation will still be performed.

All three Mg calcite sample categories (Sect. 2.1) have been implemented in PyCO2SYSv2 so the most suitable option can be chosen based on the experiment or research question. Alternatively, the user can input their own thermodynamic equilibrium constant (at standard conditions). Further, all three options for temperature dependence (Sect. 2.2) have been implemented, with the ideal solid solution (also called: ideal mix) as the default. Check values for the implementation (all three categories, all 305 temperature options under different T, S, p conditions) are given in the SI, Table S1.

2.6 Uncertainty calculation

Put together, K^* can be expressed as

$$K^* = \frac{f(K(x), T)}{\gamma_{\text{Mg}}^x \cdot \gamma_{\text{Ca}}^{1-x} \cdot \gamma_{\text{CO}_3}} \cdot \exp(-A \cdot \Delta V + 0.5 \cdot A \cdot p \cdot \Delta K) \quad (37)$$

where $K(x)$ is the result of the fit in the first step, $f(K(x), T)$ the temperature correction in step 2, and $A = \frac{P}{RT}$. The pre-310 exponent part of the equation is the calculation of K_0^* , and the exponent part is the pressure dependence to get K_p^* (which can be omitted at the surface ocean).

This equation can be used to evaluate the uncertainty σ in K^* . As a variance, this can be calculated as

$$\sigma^2(\ln K^*) = \sigma_{\ln K(x)}^2 + \sigma_{f(K(x), T)}^2 + \sigma_{\text{acf}}^2 + (A \cdot \sigma_{\Delta V})^2 + (0.5 \cdot A \cdot p \cdot \sigma_{\Delta K})^2 \quad (38)$$

We can only calculate the minimum uncertainty with the data that is available, which very likely does not represent the true 315 uncertainty because it does not capture all possible sources of error and/or because the true error cannot be evaluated with the (limited) data available.

Most measurements used in step 1 (Sect. 2.1) are not reported with an uncertainty. Thus, for step 1, the RMSE of the category 2 (with defects) fit is used for the uncertainty of $\ln K(x)$ ($\sigma_{\ln K(x)} = \text{RMSE}(\log_{10} K(x)) \cdot \ln 10$) because this category has the largest scatter in the measurements (RMSE = 0.037) and the largest spread in Mg content. The temperature dependence 320 added in step 2 shifts $K(x)$ by a certain amount. We express the uncertainty for this ($\sigma_{f(K(x), T)}$) by again using the RMSE; obtained from comparing the predicted values calculated with the three different temperature options, with the measured $\log_{10} K(x, T)$ values by Bertram et al. (1991). These RMSE values are also converted into natural log space. No exact value can be given for the uncertainty of the activity coefficients calculated with the Pitzer model (Clegg et al., 2023). Instead, we



Table 3. An overview of all the uncertainties of K^* (and Ω_{MC}) that we consider. The contribution of each of these uncertainties to the total uncertainty is also given, calculated with Eq. (39) at 10 °C.

uncertainty from	value		contribution (in %)	
	in \log_{10} space	in ln space	at 0 dbar	at 6000 dbar
K fit	0.037	0.0852	21.9	20.0
temperature corr.	0.067	0.1543	71.7	65.6
activity coefficients	0.02	0.0461	6.4	5.8
	σ	calculation		
from ΔV	$0.05 \cdot \Delta V$	$A \cdot \sigma$	0	8.5
from ΔK	$0.10 \cdot \Delta K$	$0.5 \cdot A \cdot p \cdot \sigma$	0	0.1

use the difference between $\log_{10} K_{C, \text{Mucci}}^*$ and $\log_{10} K_{C, \text{calc.}}^*$ (see Sect. 2.3), which is 0.02. Therefore, $\sigma_{\text{acf}} = 0.02 \cdot \ln 10$. All 325 these uncertainties are assumed to be independent. For the pressure correction in Step 4, we use an uncertainty of 5% for ΔV and 10% for ΔK which is line with the measurements of Ingle (1975) for calcite, resulting in $\sigma_{\Delta V} = 0.05|\Delta V|$ and $\sigma_{\Delta K} = 0.10|\Delta K|$. A summary of all these uncertainties is given in Table 3.

The contribution C of each of these terms to the total uncertainty is calculated via

$$C_i = \frac{\sigma_i^2}{\sigma^2(\ln K_p^*)} \quad (39)$$

330 To propagate this uncertainty to Ω , we assume that uncertainty of K^* is much larger than those of the concentrations of the ions in Eq. (36) and therefore $\sigma^2(\ln \Omega_{MC}) = \sigma^2(\ln K_p^*)$.

3 Results

3.1 Uncertainty

335 The fractional uncertainty of Ω is constant at the surface ocean, because it is independent of ion concentrations, salinity and, without the pressure term, of temperature. At the surface, $\sigma^2(\ln \Omega_{MC}) = 0.0332$ (Eq. 38), which is 18.2% fractional uncertainty for Ω_{MC} . The highest contribution to uncertainty stems from the temperature correction, which accounts for over 70% of this uncertainty, followed by 22% from the fit in step 1 and only about 6% stemming from the activity coefficients (Table 3). With increasing pressure the uncertainty of ΔV starts to play a role while the influence of the ΔK can be neglected but overall they do not affect the uncertainty of Ω_{MC} much. At 6000 dbar (approximately 6000 m water depth) and 10 °C, $\sigma^2(\ln \Omega_{MC}) = 0.0363$ 340 (19.0% fractional uncertainty). ΔV contributes 8.5% to this and ΔK only 0.1%.

Figure 2 shows the 1σ uncertainty for Ω_{MC} ($x = 0.14$, the average amount found in shelf sea Mg calcite sediments) with increasing pressure. Since the uncertainty is fractional, the uncertainty is larger for high values of Ω_{MC} , mainly affecting category 2 and 3 samples (all samples that are not fresh) at the surface where $\Omega_{MC} \pm 0.5$. This large uncertainty of almost

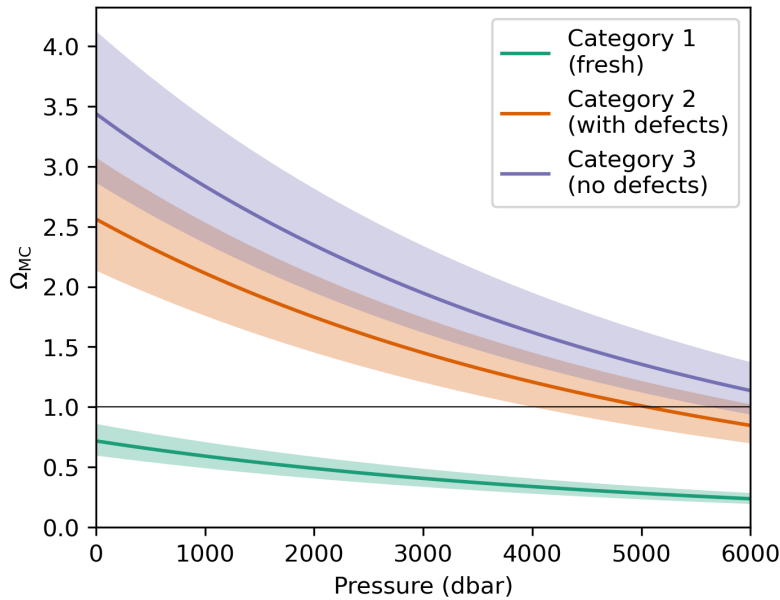


Figure 2. The 1σ uncertainty for Ω_{MC} with $x = 0.14$ at all three categories calculated with Eq. (38). The hydrographic conditions are 10°C , 35 salinity, $\text{TA} = 2300 \mu\text{mol kg}^{-1}$ and $\text{DIC} = 2100 \mu\text{mol kg}^{-1}$.

20% for Ω affects the depth of the saturation horizon substantially: for instance, whether a category 2 mineral already becomes undersaturated at ~ 4000 m or only at ~ 6000 m.

The true uncertainty for Ω may be even higher. For example, Woosley et al. (2012), one of the few studies reporting uncertainties for their solubility measurements, reported an uncertainty of 0.09 for pK^* for the solubility for a fish-produced carbonate. Assuming this uncertainty (in \ln space) for $\sigma_{\ln K(x)}$ would make that the highest contributing term (62%) and increase the total fractional uncertainty of Ω to 26% at the surface.

350 3.2 Comparison of temperature methods

Three options were implemented for the temperature dependence of K_{MC} , as shown in Fig. 3 for synthetic samples (Category 3) in comparison with the measurements by Bertram et al. (1991). For the temperature range for which they performed measurements (25 to 64°C), the ideal solid solution implementation performed the best: the RMSE for $\log_{10} K(T > 25^\circ\text{C})$ is 0.067, 0.074 and 0.081 for the ideal, van't Hoff and calcite-like implementation, respectively (see also Fig. S6). We therefore choose the ideal solid solution temperature dependence as the default. However, there is no meaningful difference between the quality of these three fits. There are not enough measurements, especially not in the temperature range where the three options deviate more significantly from each other, to clearly assess which option is superior.

The three different implementations are closest to each other between 30 and 40°C . At lower temperatures ($< 25^\circ\text{C}$) – which are more realistic for marine environments – the implementation based on van't Hoff results in the highest solubilities.

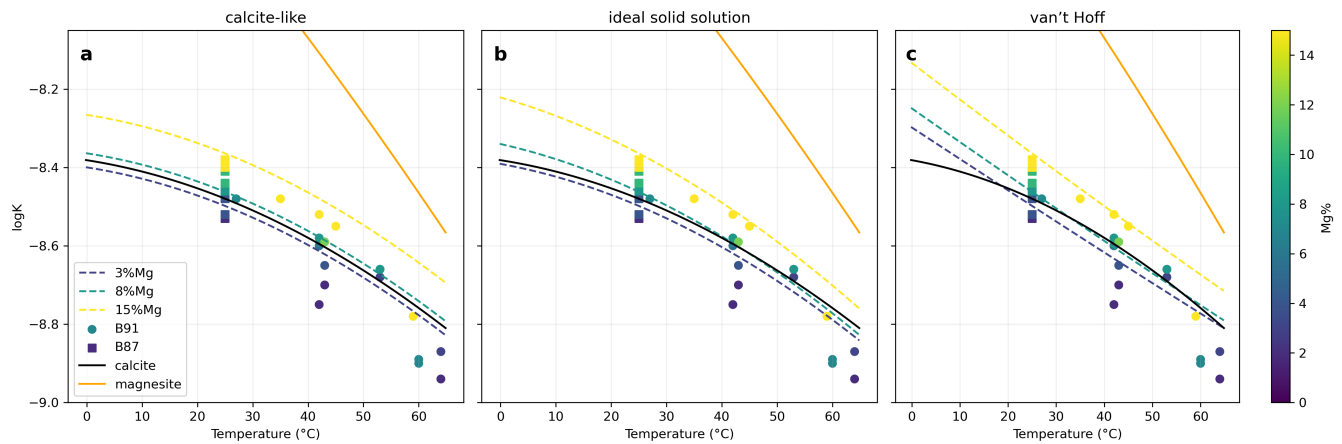


Figure 3. Temperature dependence of $\log_{10} K_{MC}$ (dashed lines), showing the three options: a) using the temperature dependence of calcite (Sect. 2.2.1), b) under the assumption of an ideal solid solution (Sect. 2.2.2) and c) calculating the temperature dependence using the van't Hoff equation (Sect. 2.2.3). Also plotted are the measurements from Bischoff et al. (1987) (B87, as squares) and Bertram et al. (1991) (B91, as circles). The temperature dependence of the solubility product of calcite (black solid line) and magnesite (orange solid line) are based on Plummer and Busenberg (1982) and Bénézeth et al. (2011), respectively.

360 For a category 2 (biogenic, with defects) Mg calcite with $x = 0.14$ (a reasonable assumption for shelf sea marine sediment) at 5 °C, $\log_{10} K_{\text{calcite-like}} = -8.16$, whereas $\log_{10} K_{\text{ideal}} = -8.13$ and $\log_{10} K_{vH} = -8.07$, which translates to 8% higher solubility for the ideal and 25% higher solubility for the van't Hoff implementation, relative to the calcite-like.

As a consequence, the chosen temperature option substantially affects the depth of the calculated saturation horizon in several ocean biomes. We calculated the saturation state for 14 Mg% (the average amount found in shelf sea carbonate sediments) 365 with all three temperature option using the GLODAPv2.2023 dataset (Lauvset et al., 2024), grouped in regional biomes (following Fay and McKinley (2014), as implemented in RECCAP2). Three biomes are highlighted in Fig. 4, and all others are found in Fig. S7. In the Subtropical North Pacific (Fig. 4a), the choice of the temperature dependence parameterisation has the smallest influence over the depth of the saturation horizon: here, the average depth for all three options falls between 600 and 700 m, which is smaller than the variability within the biome. In the Equatorial Atlantic (Fig. 4b), only with the van't Hoff 370 implementation is Mg calcite undersaturated between 500 and 1100 m before it is oversaturated again until 2200 m. With the other options, 14 Mg% calcite becomes undersaturated below 2900 m and 3300 m for the ideal solid-solution and calcite-like implementation, respectively. Since the Southern Ocean (Fig. 4c) has low seawater temperatures, which option is chosen also affects the depth of the saturation horizon more substantially. It shifts by up to 1000 m between the van't Hoff and the calcite-like implementation. However, while the different impact on the depth of the saturation horizon, the spread in Ω_{MC} at any 375 specific depth is similar for all biomes. For example, at 3000 m, Ω_{vH} is ~ 0.12 lower than Ω_{ideal} , which in turn is ~ 0.06 lower than $\Omega_{\text{ca-like}}$.

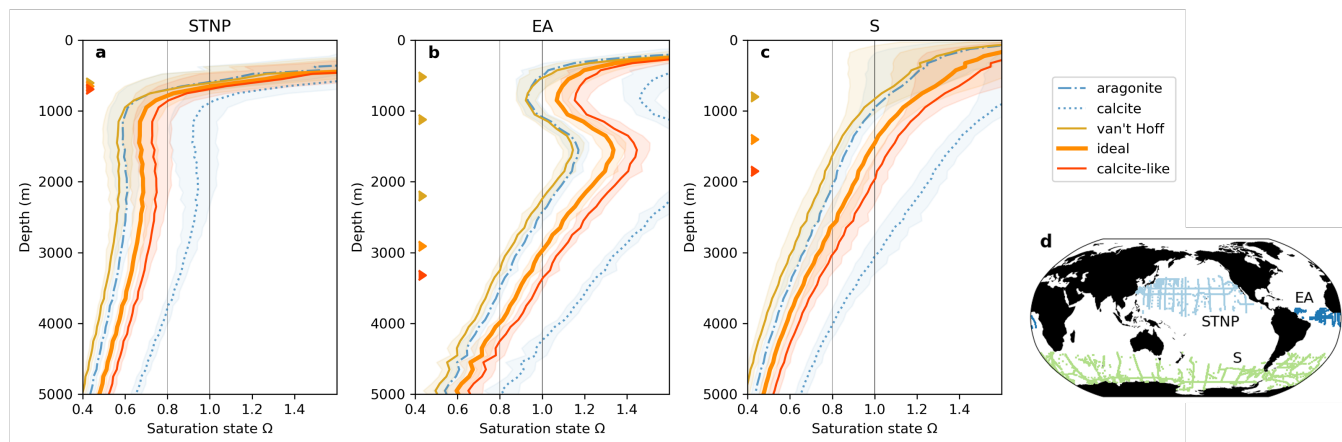


Figure 4. Saturation states with depth for the different implementations of temperature dependence of 14 Mg% (Category 2) in the (a) Subtropical North Pacific, (b) the Equatorial Atlantic and c) Southern Ocean, calculated from GLODAPv2 data. The line and envelope show the average saturation state in that ocean biome and its standard deviation. The triangles indicate the saturation horizons ($\Omega = 1$). The ocean biomes and the locations of the measurements used in this plot are shown in (d). Other oceanic regions are shown in Fig. S7.

3.3 Global saturation states

Mg calcite saturation states (using the ideal solid solution option for temperature dependence) for the global surface ocean have been calculated with temperature, salinity and $[CO_3^{2-}]$ data from OceanSODA-ETHZ (Gregor and Gruber, 2021). Only data 380 for the year 2022 were used, and the various monthly saturation states were calculated and then averaged. The surface ocean was oversaturated for almost all types of Mg calcite, except for category 1 (fresh) with a higher Mg content than 10% (Fig. 5). Category 3 (no defects) Mg calcites up to ~ 15 Mg% were more oversaturated at the surface than calcite is and category 2 (with defects) Mg calcites were globally less oversaturated than calcite but more oversaturated than aragonite until at least 20 Mg%.

Figures 6 and 7 show Ω_{MC} along meridional transects across the Atlantic and Pacific Oceans, respectively. The saturation 385 states were calculated from TA and DIC as input parameters in PyCO2SYS (version 2.0.0-b5) (Humphreys et al., 2025), using Lueker et al. (2000) for the carbonic acid dissociation constants, the boron:chlorinity relationship of Uppström (1974), the calcite:salinity relationship of Riley and Tongudai (1967), the magnesium:salinity relationship of Millero et al. (2008), and all other default equilibrium constants.

The biggest change in saturation horizon with increasing x is in category 1 (fresh) where the saturation horizon is between 390 3000 and 4000 m at $x = 0.05$ and becomes almost 0 m at $x = 0.15$. For the other two categories the depth of the saturation horizon varies only by ~ 1500 m. For Category 3 (no defects, synthetic), the saturation horizon is below that of calcite until 10 Mg% and is never shallower than that of aragonite. For category 2 (with defects, biogenic), only at $x = 0.20$ does the saturation horizon of Mg calcite lie above the aragonite saturation horizon. Category 1 (fresh) is the only solubility implementation where Mg calcite is more undersaturated than aragonite in the most relevant range of Mg, between 10 and 18 Mg%.

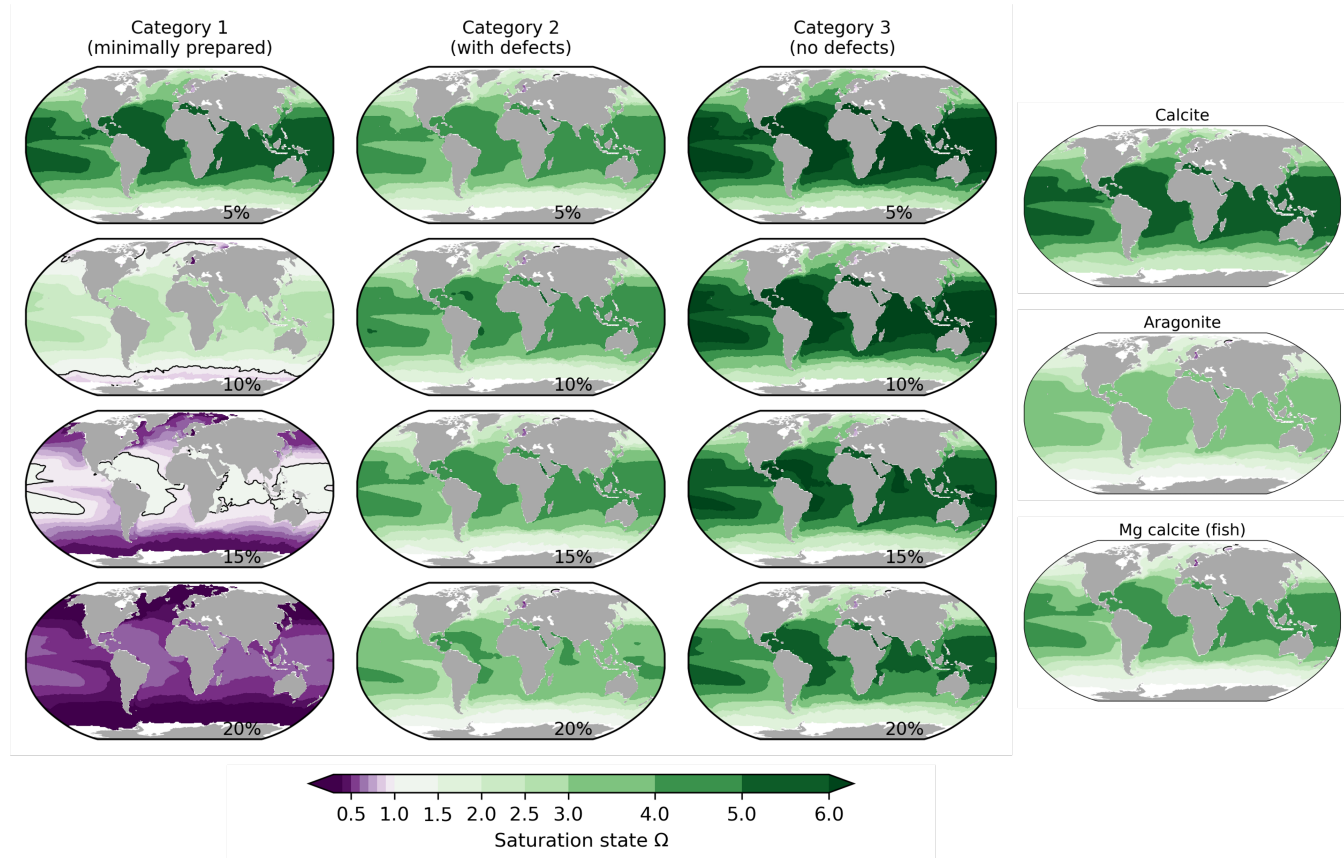


Figure 5. Annual average of the surface saturation states with respect to calcite, aragonite and Mg calcite with different Mg content, calculated from the OceanSODA-ETHZ data product for the year 2022.

395 4 Discussion

4.1 Case study: fish-produced Mg calcite

For calcite and aragonite, the saturation state is calculated with Eq. (1). However, for Mg calcites this equation would assume that Ω_{MC} is independent of the the Mg^{2+} concentration in seawater. The equilibrium constant K is best expressed by $a(Ca^{2+})^{1-x} \cdot a(Mg^{2+})^x \cdot a(CO_3^{2-})$ and not $a(Ca^{2+}) \cdot a(CO_3^{2-})$ (Walter and Morse, 1984), so it makes sense to apply this to Ω too and use Eq. (36) instead of Eq. (1) to calculate saturation states. Because the concentration of Mg^{2+} in the modern ocean is 5 times that of Ca^{2+} , the saturation state with respect to Mg calcite is often higher for Mg calcites than for aragonite, even though it is more soluble (i.e. higher K). This has been neglected in some studies (Woosley et al., 2012; Sulpis et al., 2021; Hashim et al., 2025).

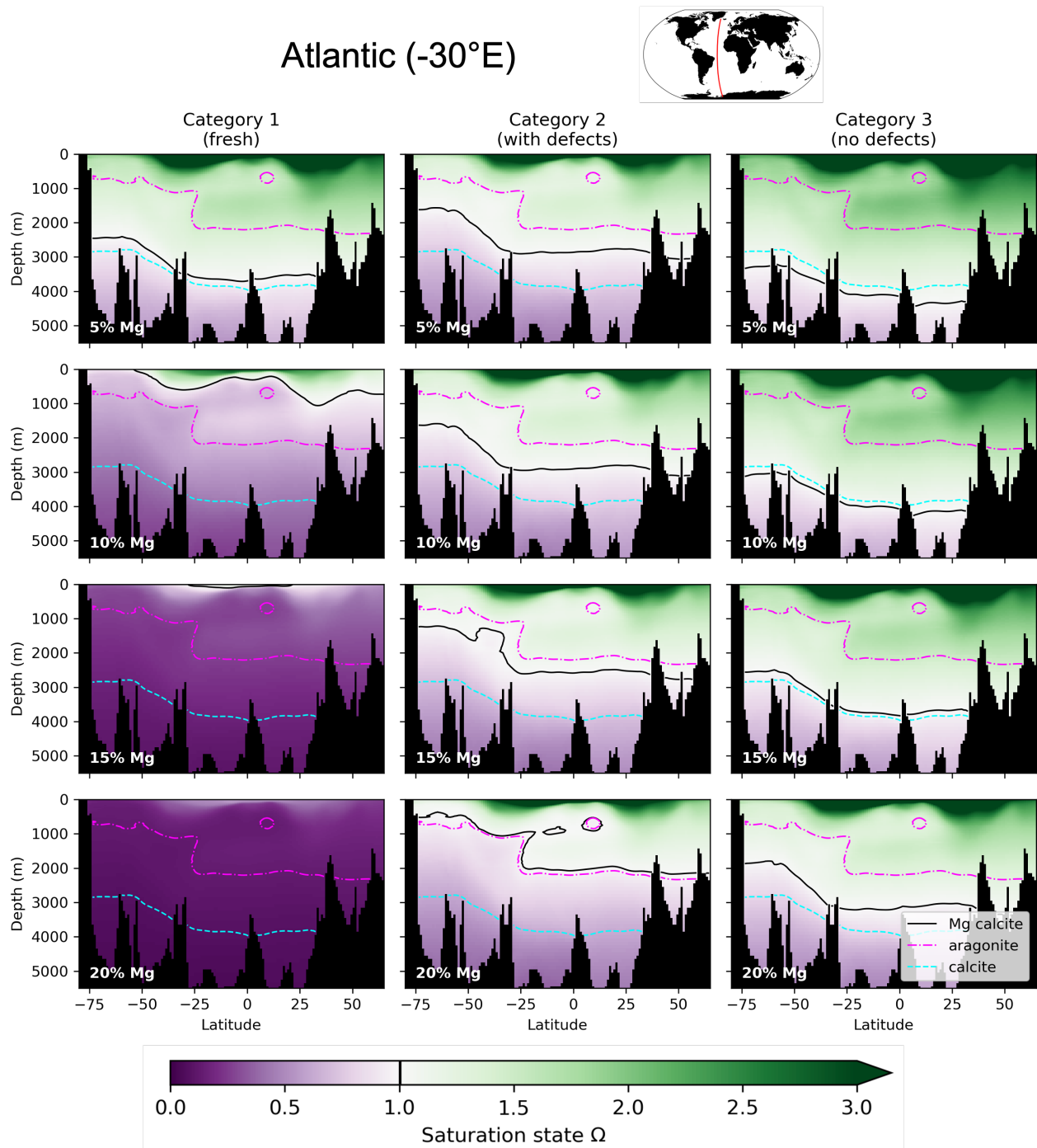


Figure 6. Saturation states along a transect in the Atlantic (-30° E). Each column is one category (Fig. 1) Mg content is increasing down each column (5%, 10%, 15% and 20%). The saturation horizon ($\Omega = 1$) is shown as a black line for the Mg calcite, a dash-dotted pink line for aragonite and a dashed cyan line for calcite.



Pacific (-150°E)

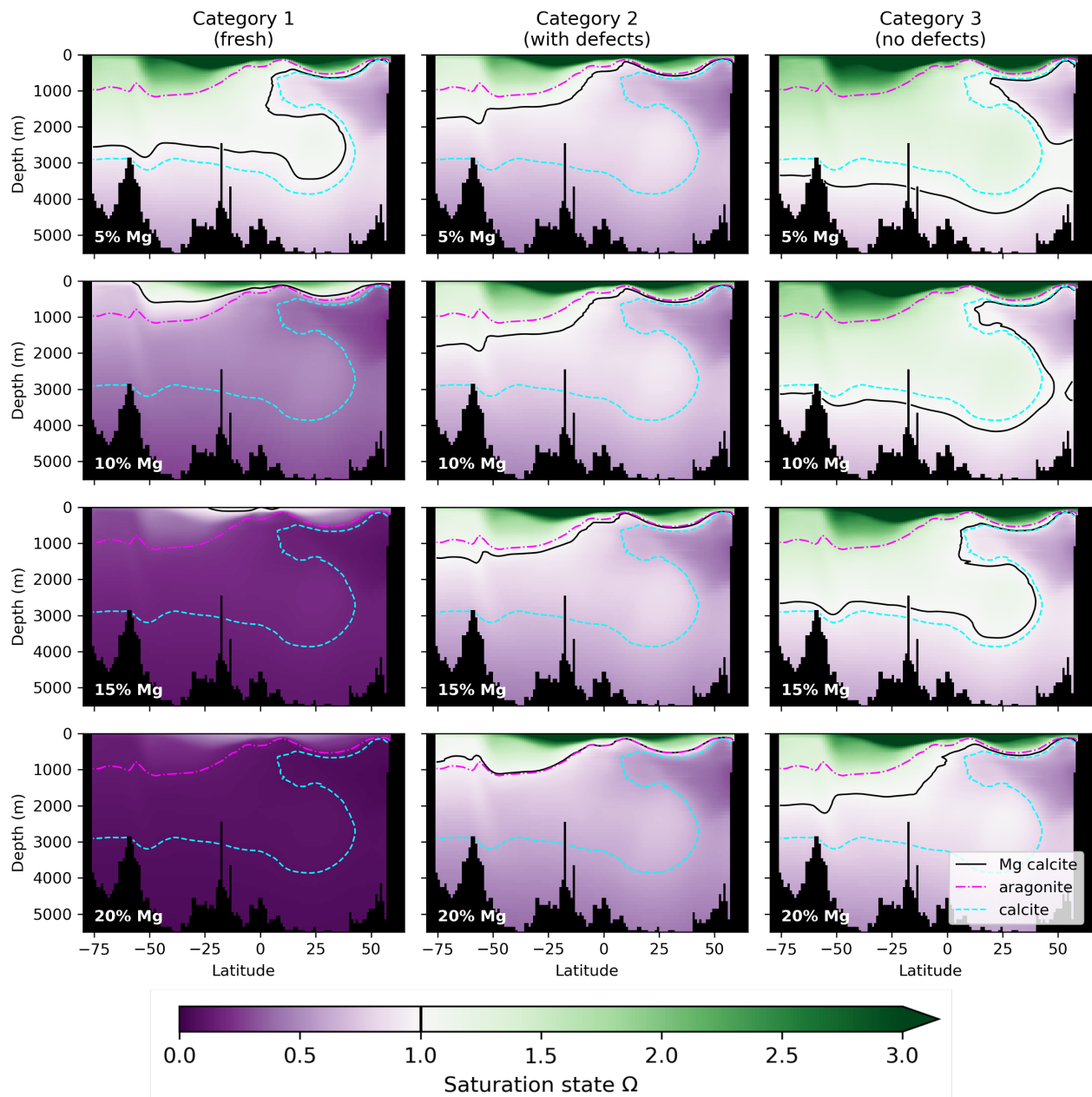
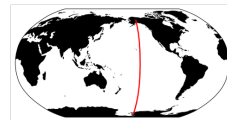


Figure 7. Saturation states along a transect in the Pacific (-150°E). Each column is one category (Fig. 1) and Mg content is increasing down each column (5%, 10%, 15% and 20%). The saturation horizon ($\Omega = 1$) is shown as a black line for the Mg calcite, a dash-dotted pink line for aragonite and a dashed cyan line for calcite.



We illustrate the importance of this concept with the fish-produced carbonate minerals (ichthyocarbonates). Due to their
405 their high Mg content and therefore their high solubility, it has been proposed that they could dissolve high in the water column
and could thus help to close the gap in alkalinity (Wilson et al., 2009; Woosley et al., 2012; Oehlert et al., 2024a).

The only direct solubility study of ichthyocarbonates is by Woosley et al. (2012), who measured the solubility of bleached
fish-produced Mg calcite of the gulf toadfish kinetically with extrapolation to infinite time. The Mg content was $47.9\% \pm 0.7$
and the stoichiometric equilibrium constant was reported as $pK^*((25^\circ\text{C}, S = 36.5, 1\text{ atm}) = 5.89(\pm 0.09)$, which is 1.95 times
410 more soluble than aragonite. Subsequent studies have used this measurement directly to calculate the depth of the saturation
horizon of fish-produced Mg calcite. Sulpis et al. (2021) used $pK^*((25^\circ\text{C}, S = 36.5, 1\text{ atm}) = 5.89$ as an input to Eq. (1),
without considering temperature or pressure effects. They reported an average depth of 200 to 900 m for the saturation horizon
in the different regional ocean biomes (Fig. 2, *ibid.*). Woosley et al. (2012) and Hashim et al. (2025) calculated the solubility
with

$$415 \quad \Omega_{\text{fish}}(T, S, p) = \Omega_A(T, S, p) \cdot \frac{K_A^*(25^\circ\text{C}, 1\text{ atm})}{K_{\text{fish}}^*(25^\circ\text{C}, 1\text{ atm})} \quad (40)$$

relying on the assumptions that Mg calcite is 1.95 times more soluble than aragonite and the saturation state with respect to
Mg calcites can also be computed with Eq. (1). In Woosley et al. (2012), the saturation horizons have a depth between 0 and
500 m (the Southern Ocean is on average completely undersaturated) and Hashim et al. (2025) calculated a saturation horizon
of 800 m for the site of the Bermuda Atlantic Time Series (BATS). Based on these results, ichthyocarbonates could indeed
420 explain some of the shallow carbonate mineral dissolution.

Using our implementation, we calculated saturation horizon depths with Eq. (36), taking into account Mg^{2+} concentration.
For this, we converted the measurement of the stoichiometric equilibrium constant K^* by Woosley et al. (2012) to the
thermodynamic equilibrium constant $K(25^\circ\text{C}, 1\text{ atm})$ with Eq. (24), by calculating the activity coefficients with Pytzer, as
already described in Sect. 2.3. This resulted in $pK(25^\circ\text{C}, 1\text{ atm}) = 7.98(\pm 0.09)$ (Fig. 1). This value was used as an input for
425 PyCO2SYS which then carried out the temperature and pressure correction of K before calculating Ω_{fish} .

In the Subtropical North Pacific and Southern Ocean we calculate an average saturation horizon depth of 600 m and 700 m,
respectively, which is not far off the values calculated by Sulpis et al. (2021). However, in the Subtropical North Atlantic, the
saturation horizon lies at 2200 m (Fig. S8). At the BATS location, the ichthyocarbonate saturation horizon is also at or below
2000 m (Fig. S9, using the bottle data from the BATS validation cruises 1991 to 2024 (Bates et al., 2025)). In all instances, the
430 ichthyocarbonate saturation horizon depth is only 10 to 300 m above the aragonite saturation horizon and Ω_{fish} is only ~ 0.1
lower compared to Ω_A (see also Fig. 5 where Ω_{fish} is even higher than Ω_A in the surface ocean). Our calculations make it seem
less likely that ichthyocarbonates could contribute globally to shallow dissolution (< 1000 m).

However, these estimates of solubility (thermodynamic) are inconsistent with ichthyocarbonate dissolution rate measurements
(kinetic) (Folkerts et al., 2024). Dissolution rates were measured for ichthyocarbonates produced from three different
435 marine fish (including the gulf toadfish) and found signs of dissolution at $\Omega_A > 1.5$ (Ω_{MC} could not be calculated since those
data are not freely available). Organic coatings of these (fresh) samples could in principle explain the higher solubility com-
pared to the bleached samples of Woosley et al. (2012) (analogous to category 1 (fresh) also having a higher solubility than



category 2 (with defects)) but Oehlert et al. (2024b) showed that organic coatings actually reduce the dissolution rate for ichthyocarbonates, suggesting the opposite effect to be true here. It is unclear whether this discrepancy between thermodynamic and 440 kinetic data stems from problems in the solubility implementation in this work, the measurements themselves or simply from sample heterogeneity.

4.2 Case study: Mg calcite ooids

Most in situ dissolution rate measurements in the water column have been focused on calcite and aragonite (Cala et al., 2024). However, a single study also used 12 Mg% calcite ooids (Milliman, 1977). Ooids are small, round sedimentary grains that can 445 form at the seafloor in warm, shallow water. They were placed on a mooring for 9 months at three locations in the Sargasso Sea at 8 to 10 depths between 1000 and 5000 m (a fourth station is excluded in the analysis here because its experimental setup differed from the other three stations). At all three stations, the measured dissolution rate for the Mg calcite ooids was slower than that of aragonite ooids. Both types of samples were of similar size (250 to 500 µm) and prepared in the same way. We therefore assume that the difference in dissolution rate did not stem from the experimental setup but mainly from the different 450 saturation states that the samples experienced due to differences in their solubility, meaning, that the kinetic measurements can be used as a proxy for thermodynamic solubility.

Calculating saturation states for $x = 0.12$ for all three categories (using the default option for temperature dependence, ideal mix and using the salinity (for $[Ca^{2+}]$) and TA and DIC values (for $[CO_3^{2-}]$) from Cala et al. (2024)), reveals that the solubility of category 2 (with defects) can model the dissolution behaviour the best (Fig. 8), as was expected from the sample description 455 (Figs. S10 and S11 show the results for the other two implemented temperature options). The saturation horizon depth was at ~ 3300 m where the Mg calcite ooids showed the first sign of dissolution and it passed $\Omega_{crit} = 0.8$ at ~ 4500 m, which is where for aragonite and calcite the dissolution mechanism changes and the dissolution rate starts to increase more rapidly with depth and decreasing Ω (Naviaux et al., 2019). For the Mg calcite ooids the rate also seems to have started to increase there more rapidly. The dissolution rate of calcite and aragonite is often fitted to:

$$460 \quad r = k(1 - \Omega)^n \quad (41)$$

where k is the rate constant and n the reaction order. Walter and Morse (1984) found that Mg calcite had a similar reaction order to calcite and aragonite ($n \approx 3$). When plotted against the calculated Ω , Mg calcite should therefore exhibit a similar dissolution behaviour as the aragonite samples. Figure 8c shows that this is the case: The data points of category 2 Mg calcite lie directly above the measurements for aragonite (this also is the case for the calcite-like temperature implementation (Fig. S10c) but not 465 for the van't Hoff temperature option (Fig. S11c)).

The implementation of Mg calcite solubility presented here can provide a satisfactory explanation of the in situ dissolution rate measurements by Milliman (1977). However, this has several limitations. Since the dissolution rate was solely determined via weight loss, it cannot be ruled out that incongruent dissolution took place throughout deployment and (lower Mg) calcite precipitated again on the Mg calcite ooids, thus lowering weight loss and the calculated dissolution rate. Additionally, it is 470 unknown whether Mg was homogeneously distributed in the samples or whether the dissolving phase had a higher Mg content.

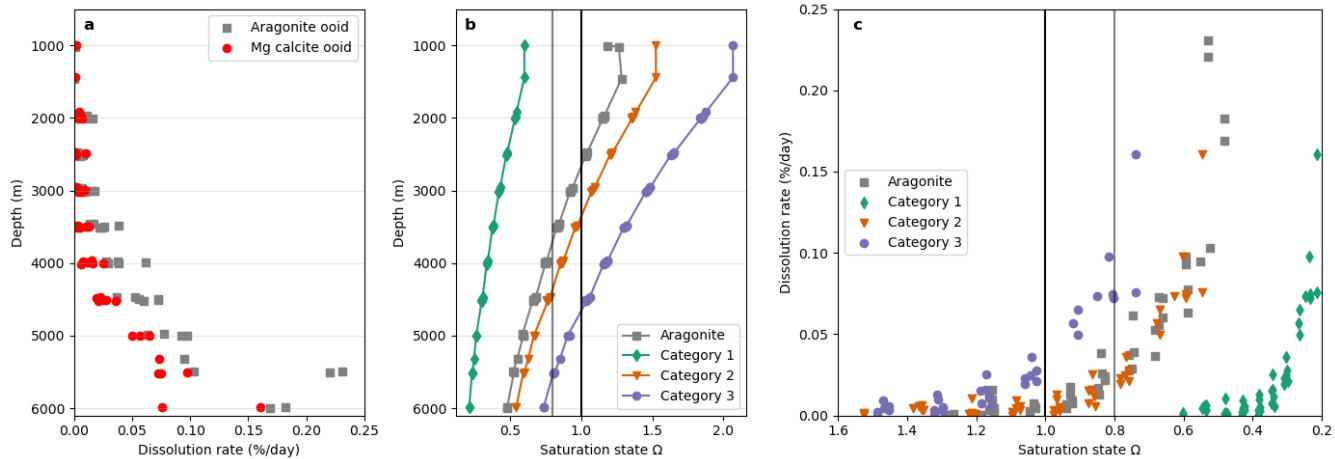


Figure 8. Subplot (a) shows the combined dissolution rate measurements from three stations by Milliman (1977) against depth. In (b) the saturation state for aragonite and all three solubility categories with $x = 0.12$ is plotted against depth (ideal mix temperature option) and (c) shows the measured dissolution rate against the calculated Ω .

Finally, incorrect assumptions for the parameterisation of temperature and pressure dependence could have led to this result by chance. More field experiments with different Mg calcites are needed to further investigate the validity of this implementation.

4.3 Global biogeochemical implications

Evaluating the implications of Mg calcite solubility to the carbon cycle is challenging. There are many unknowns both about the (i) dissolution behaviour of Mg calcites and (ii) its production and distribution in the ocean.

(i) Uncertainty about which category represents dissolution best in the real ocean limits our ability to predict which minerals are already undersaturated or when and where they will become so. Dissolution behaviour of different Mg calcites with rising $p\text{CO}_2$ has already been investigated in more detail in a box model study of a shelf sea by Morse et al. (2006). They reported that category 1 (fresh) Mg calcites already showed dissolution of 18% Mg calcite under current ocean conditions at a water depth of 130 m. However, for category 2 (biogenic, with defects), 18% Mg calcite would only start to become undersaturated at the same depth in over 200 years, when $p\text{CO}_2 > 1400$ ppm. This shows the large effect that the category has on dissolution. Additional complexities arise from the possibility that after initial dissolution particles of category 1 (fresh) can be stabilised into category 2 but the necessary conditions and the timescale of this process are unknown (Bischoff et al., 1993). The large uncertainty associated with the temperature dependence of Mg calcite solubility further amplifies the problem of dissolution behaviour in the natural environment.

(ii) How Mg calcites of different Mg contents are distributed globally is poorly known. Even though they are more extensively studied, there are still large uncertainties about calcite and aragonite production, and this is equally or more true for Mg



calcites. Recently, Pedrosa-Pamies et al. (2025) showed that hurricanes around Bermuda play a significant role in the sediment resuspension and offshore advective transport by internal waves. This process may contribute to the delivery of Mg calcite to
490 the open ocean, even though not much is produced there in situ. Some particles might stay resuspended, dissolve in the water column contribute to shallow dissolution, alongside biologically mediated dissolution in zooplankton guts or organic matter degradation. Others might get repackaged (e.g., into fecal pellets) and sink quickly to the seafloor. At the surface-sediment interface, Mg calcites could fulfil a similar role as aragonite by protecting calcite from dissolution (Sulpis et al., 2022). However, the relevance of these processes cannot be assessed without more knowledge of Mg calcite production and spatial distribution.

495 4.4 Recommended use cases

Mg content alone is insufficient to describe the solubility of various biogenic and synthetic Mg calcite phases, as the solubility depends on crystal-level factors (e.g. cation ordering, defect density, incorporation of foreign ions and microstructure) but also on macroscopic variables, such as sample treatment (e.g. cleaning procedures). The available solubility measurements can be grouped into three categories but for many samples or research questions it may be unclear which category fits best. In some
500 cases, a sample may not be well represented by any of these standard categories (e.g. ichthyocarbonates).

The solubility of "fresh" samples, i.e. dead organisms sinking through the water column or organisms removed from an aquarium that have not been cleaned at all to remove organic coatings or highly reactive particles on the surface might best be described by category 1.

The solubility of biogenic samples from the water column or aquarium that underwent some cleaning procedure should
505 probably be calculated with category 2. The same goes for biogenic samples collected from marine sediments, as organic material has likely been degraded and the most reactive parts already dissolved. Based on the results presented in Sect. 4.2, high Mg calcite ooids and cements might also be best represented by category 2. However, this might be dependent on the amount of foreign ions incorporated in the mineral.

Most synthetic samples, especially when slowly grown and low concentration of foreign ions in the aqueous solution, have
510 a low defect density. Their solubility will most likely be best described by category 3.

Ichthyocarbonates are probably not well represented in any of these categories based on their high Mg contents and the experimental results of Woosley et al. (2012). Instead, the single solubility measurement can be extrapolated towards different temperatures and pressures as done in Sect. 4.1 by calculating the thermodynamic equilibrium constant and then accounting for temperature and pressure effects. This measurement is closest to other measurements in category 2 (with defects), however,
515 there is such little data at such high Mg contents that a comparison is not feasible. Due to the large diversity in ichthyocarbonates, this value might be very different for another species even if it is the same Mg content or even the same species at a different Mg content. Additionally, it is unknown if the solubility may be different for fresh samples with organics still present. Because the dissolution rate is reduced by organic coatings (Oehlert et al., 2024b), this could hint at lower solubility which would be the opposite behaviour than what is seen for categories 1 and 2 (fresh and with defects).

520 For temperature correction, the ideal solid solution implementation is the default option because it gave slightly better results when comparing against the measurements of Bertram et al. (1991) and was able to reproduce the dissolution behaviour of



aragonite when applied to Mg calcite ooid dissolution rate data by Milliman (1977). However, because it wasn't possible to meaningfully determine which option is best with the data available, we recommend trying all three options and comparing the results.

525 5 Conclusions

The implementation of Mg calcite solubility presented in this work hinges on several assumptions. For example, we assume that pressure dependence is similar to calcite and aragonite, despite the smaller ionic radius of Mg^{2+} compared to Ca^{2+} . In many cases, we assume an ideal solid solution between calcite and magnesite; however, it remains unclear whether this simplification is sufficient to yield realistic solubilities for Mg calcite.

530 By contrast, the implementation of calcite and aragonite solubility by Mucci (1983) is based on parameterisations of measurements across a range of conditions. Even though comparable experiments might not be feasible for the full range of Mg contents, more limited experiments would still be valuable. Specifically, solubility measurements for at least two different Mg calcites could be conducted for temperatures between 0 and 25 °C to test which temperature implementation of the three presented here is most accurate or if another parameterisation is required. Similar data are needed to verify the validity of the 535 applied pressure correction.

Since fish-produced Mg calcite and its role in the carbonate Additional uncertainties exist for fish-produced Mg calcite, which has become a focus in the last two decades due to its role in the carbonate pump. For instance, kinetic dissolution rates seem to contradict the thermodynamic predictions from this study: Oehlert et al. (2024b) model that ichthyocarbonate samples up to 0.91 mm from the gulf toadfish will be completely dissolved at a depth of 348 m, whereas we calculate a saturation 540 horizon below 500 m. Therefore, better constraints for fish carbonate solubility are needed, how it differs between and within species and for different sample treatments. Following the example of Hashim et al. (2025), additional studies could investigate the presence of fish-produced Mg calcite in sediment traps of various depths, especially in regions with high fish biomass.

In situ particle dissolution rate measurements on moorings (such as Milliman (1977) conducted for Mg calcite ooids) could further verify the proposed implementation because they are able to cover a wide range of pressure and lower temperatures. 545 Biogenic samples (e.g. benthic foraminifera, sea urchins, coralline algae, stony corals, ichthyocarbonates) would be useful samples for this experiment, ideally with as little sample treatment before deployment as possible. This could also help assess the fate of Mg calcites from shallow shelf seas that are resuspended and moved to deeper waters.

While many unknowns remain, this work still is a step forward. Our implementation provides a clear improvement to the solubility curves (that show the ion activity product at equilibrium for different Mg contents at standard conditions, Fig. 1) and 550 which so far have been the basis for discussions around Mg calcite solubility, by incorporating a temperature, salinity and pressure dependence. We also improve on previous studies by correctly accounting for Mg^{2+} concentration when calculating Ω_{MC} . Implementing this in (parts of) the already widely used CO2SYS software family, makes the calculation of the Mg calcite saturation state under different conditions as straightforward as for calcite and aragonite, albeit with greater uncertainty. We show



that the largest uncertainties for the calculation of Ω_{MC} lie in how real world Mg samples are categorised and the temperature 555 dependence of K ; studies focusing on these two issues would yield the greatest improvements to our understanding.

Code and data availability. The code that generated all figures and was used to create the implementation and conduct all analysis can be found at <https://github.com/bcalal/Mg-calcite> (Cala, 2025). The implementation of Mg calcite solubility is implemented in version v2.0.0-b5 (Humphreys et al., 2025) and all future versions. Activity coefficients were modelled with Pytzer version v0.6.0 (Humphreys and Schiller, 2024). The data used for the $K(x)$ fits (Step 1) is listed in Table 1. The OceanSODA-ETHZ data set can be found at Gregor and Gruber 560 (2020) and GLODAPv2.2023 at Lauvset et al. (2023). The data used in Sect. 4.2 is from Milliman (1977) and Cala and Humphreys (2024).

Author contributions. CRediT: BAC: Conceptualization, Data curation, Formal Analysis, Investigation, Methodology, Software, Validation, Visualization, Writing (original draft), Writing (review and editing); MW: Conceptualization, Funding acquisition, Methodology, Supervision, Writing (review and editing); OS: Funding acquisition, Supervision, Writing (review and editing); JDS: Software, Validation, Writing (review and editing); MPH: Conceptualization, Funding acquisition, Methodology, Software, Supervision, Validation, Writing (review and 565 editing)

Competing interests. Some authors are members of the editorial board of Ocean Science.

Acknowledgements. The authors would like thank all the scientists and technicians over the last seven decades who conducted the solubility measurements of carbonate minerals on which this work relies on. This research was funded by the UU-NIOZ collaboration project, “BEYΩND the known drivers of marine carbonate mineral dissolution: closing the gap in the alkalinity budget”. This project has received 570 funding from the European Research Council (ERC) under the European Union’s Horizon 2020 research and innovation programme (grant agreement No. [819588]). OS was supported by the Netherlands Organization for Scientific Research (NWO-VENI Grant VI.Veni.212.086). JDS was supported by the Cooperative Institute for Climate, Ocean, & Ecosystem Studies (CIOCES) under NOAA cooperative agreement no. NA20OAR4320271; this is CICOES contribution no. xxx and NOAA PMEL contribution no. xxx (CONTRIBUTION NUMBERS WILL BE ADDED LATER).



575 **References**

- Agegian, C. R.: The Biogeochemical Ecology of Porolithon Gardineri(Foslie), Ph.D. thesis, University of Hawaii Honolulu, 1985.
- Agegian, C. R. and Mackenzie, F. T.: Calcareous Organisms and Sediment Mineralogy on a Mid-Depth Bank in the Hawaiian Archipelago, Pacific Science, 43, 56–66, 1989.
- Althoff, P. L.: Structural Refinements of Dolomite and a Magnesian Calcite and Implications for Dolomite Formation in the Marine Environment, American Mineralogist, 62, 772–783, 1977.
- Andersson, A., Mackenzie, F., and Bates, N.: Life on the Margin: Implications of Ocean Acidification on Mg-calcite, High Latitude and Cold-Water Marine Calcifiers, Mar. Ecol. Prog. Ser., 373, 265–273, <https://doi.org/10.3354/meps07639>, 2008.
- Bates, N., Johnson, R. J., Lomas, M. W., Carlson, C. A., Smith, D., Lethaby, P. J., Lomas, D., Medley, C., May, R., Davey, E., Stuart, E., Garley, R., and Derbyshire, L.: Discrete Bottle Samples Collected during BATS Validation (BVAL) Cruises from April 1991 through July 2024, <https://doi.org/10.26008/1912/BCO-DMO.917255.7>, 2025.
- Bénézeth, P., Saldi, G. D., Dandurand, J.-L., and Schott, J.: Experimental Determination of the Solubility Product of Magnesite at 50 to 200 °C, Chemical Geology, 286, 21–31, <https://doi.org/10.1016/j.chemgeo.2011.04.016>, 2011.
- Berelson, W. M., Balch, W. M., Najjar, R., Feely, R. A., Sabine, C., and Lee, K.: Relating Estimates of CaCO₃ Production, Export, and Dissolution in the Water Column to Measurements of CaCO₃ Rain into Sediment Traps and Dissolution on the Sea Floor: A Revised Global Carbonate Budget, Global Biogeochemical Cycles, 21, <https://doi.org/10.1029/2006GB002803>, 2007.
- Bertram, M. A., Mackenzie, F. T., Bishop, F. C., and Bischoff, W. D.: Influence of Temperature on the Stability of Magnesian Calcite, American Mineralogist, 76, 1889–1896, 1991.
- Bischoff, W. D.: Magnesian Calcites: Physical and Chemical Properties and Stabilities in Aqueous Solution of Synthetic and Biogenic Phases (Carbonates, Solid Solutions), Ph.D. thesis, Northwestern University, 1985.
- Bischoff, W. D.: Dissolution Enthalpies of Magnesian Calcites, Aquatic Geochemistry, 4, 321–336, <https://doi.org/10.1023/A:1009684214945>, 1998.
- Bischoff, W. D., Mackenzie, F. T., and Bishop, F. C.: Stabilities of Synthetic Magnesian Calcites in Aqueous Solution: Comparison with Biogenic Materials, Geochimica et Cosmochimica Acta, 51, 1413–1423, [https://doi.org/10.1016/0016-7037\(87\)90325-5](https://doi.org/10.1016/0016-7037(87)90325-5), 1987.
- Bischoff, W. D., Bertram, M. A., Mackenzie, F. T., and Bishop, F. C.: Diagenetic Stabilization Pathways of Magnesian Calcites, Carbonates and Evaporites, 8, 82–89, <https://doi.org/10.1007/BF03175165>, 1993.
- Busenberg, E. and Plummer, L. N.: Thermodynamics of Magnesian Calcite Solid-Solutions at 25°C and 1 Atm Total Pressure, Geochimica et Cosmochimica Acta, 53, 1189–1208, [https://doi.org/10.1016/0016-7037\(89\)90056-2](https://doi.org/10.1016/0016-7037(89)90056-2), 1989.
- Cala, B.: bcalal/Mg-calcite: Version 0.1 – Initial release (manuscript submission), <https://doi.org/10.5281/zenodo.17342280>, 2025.
- Cala, B. A. and Humphreys, M. P.: Synthesis of In Situ Marine Calcium Carbonate Dissolution Kinetic Measurements in the Water Column - Data, <https://doi.org/10.25850/nioz/7b.b.bg>, 2024.
- Cala, B. A., Sulpis, O., Wolthers, M., and Humphreys, M. P.: Synthesis of In Situ Marine Calcium Carbonate Dissolution Kinetic Measurements in the Water Column, Global Biogeochemical Cycles, 38, e2023GB008 009, <https://doi.org/10.1029/2023GB008009>, 2024.
- Chave, K. E.: Aspects of the Biogeochemistry of Magnesium 2. Calcareous Sediments and Rocks, The Journal of Geology, 62, 587–599, <https://doi.org/10.1086/626208>, 1954.
- Chave, K. E., Deffeyes, K. S., Weyl, P. K., Garrels, R. M., and Thompson, M. E.: Observations on the Solubility of Skeletal Carbonates in Aqueous Solutions, Science, 137, 33–34, <https://doi.org/10.1126/science.137.3523.33>, 1962.



- Clegg, S. L., Waters, J. F., Turner, D. R., and Dickson, A. G.: Chemical Speciation Models Based upon the Pitzer Activity Coefficient Equations, Including the Propagation of Uncertainties. III. Seawater from the Freezing Point to 45 °C, Including Acid-Base Equilibria, *Marine Chemistry*, 250, 104 196, <https://doi.org/10.1016/j.marchem.2022.104196>, 2023.
- 615 Dong, S., Pavia, F. J., Subhas, A. V., Gray, W. R., Adkins, J. F., and Berelson, W. M.: Carbon Cycling in Marine Particles Based on Inorganic and Organic Stable Isotopes, *Geochimica et Cosmochimica Acta*, 388, 208–220, <https://doi.org/10.1016/j.gca.2024.10.005>, 2025.
- Fay, A. R. and McKinley, G. A.: Global Open-Ocean Biomes: Mean and Temporal Variability, *Earth System Science Data*, 6, 273–284, <https://doi.org/10.5194/essd-6-273-2014>, 2014.
- Folkerts, E. J., Oehlert, A. M., Heuer, R. M., Nixon, S., Stieglitz, J. D., and Grosell, M.: The Role of Marine Fish-Produced Carbonates in the 620 Oceanic Carbon Cycle Is Determined by Size, Specific Gravity, and Dissolution Rate, *Science of The Total Environment*, 916, 170 044, <https://doi.org/10.1016/j.scitotenv.2024.170044>, 2024.
- Friedlingstein, P., O'Sullivan, M., Jones, M. W., Andrew, R. M., Hauck, J., Landschützer, P., Le Quéré, C., Li, H., Luijkx, I. T., Olsen, A., Peters, G. P., Peters, W., Pongratz, J., Schwingshackl, C., Sitch, S., Canadell, J. G., Ciais, P., Jackson, R. B., Alin, S. R., Arneth, A., Arora, V., Bates, N. R., Becker, M., Bellouin, N., Berghoff, C. F., Bittig, H. C., Bopp, L., Cadule, P., Campbell, K., Chamberlain, M. A., 625 Chandra, N., Chevallier, F., Chini, L. P., Colligan, T., Decayeux, J., Djetchouang, L. M., Dou, X., Duran Rojas, C., Enyo, K., Evans, W., Fay, A. R., Feely, R. A., Ford, D. J., Foster, A., Gasser, T., Gehlen, M., Gkritzalis, T., Grassi, G., Gregor, L., Gruber, N., Gürses, Ö., Harris, I., Hefner, M., Heinke, J., Hurtt, G. C., Iida, Y., Ilyina, T., Jacobson, A. R., Jain, A. K., Jarníková, T., Jersild, A., Jiang, F., Jin, Z., Kato, E., Keeling, R. F., Klein Goldewijk, K., Knauer, J., Korsbakken, J. I., Lan, X., Lauvset, S. K., Lefèvre, N., Liu, Z., Liu, J., Ma, L., Maksyutov, S., Marland, G., Mayot, N., McGuire, P. C., Metzl, N., Monacci, N. M., Morgan, E. J., Nakaoka, S.-I., Neill, C., Niwa, Y., 630 Nützel, T., Olivier, L., Ono, T., Palmer, P. I., Pierrot, D., Qin, Z., Resplandy, L., Roobaert, A., Rosan, T. M., Rödenbeck, C., Schwinger, J., Smallman, T. L., Smith, S. M., Sospedra-Alfonso, R., Steinhoff, T., Sun, Q., Sutton, A. J., Séférian, R., Takao, S., Tatebe, H., Tian, H., Tilbrook, B., Torres, O., Tourigny, E., Tsujino, H., Tubiello, F., van der Werf, G., Wanninkhof, R., Wang, X., Yang, D., Yang, X., Yu, Z., Yuan, W., Yue, X., Zaehle, S., Zeng, N., and Zeng, J.: Global Carbon Budget 2024, *Earth System Science Data*, 17, 965–1039, <https://doi.org/10.5194/essd-17-965-2025>, 2025.
- 635 Garrels, R. and Wollast, R.: Equilibrium Criteria for Two-Component Solids Reacting with Fixed Composition in an Aqueous Phase; Example, the Magnesian Calcites; Discussion, *American Journal of Science*, 278, 1469–1474, <https://doi.org/10.2475/ajs.278.10.1469>, 1978.
- Gregor, L. and Gruber, N.: OceanSODA-ETHZ: A Global Gridded Dataset of the Surface Ocean Carbonate System for Seasonal to Decadal Studies of Ocean Acidification (V2023) (NCEI Accession 0220059), <https://doi.org/10.25921/M5WX-JA34>, 2020.
- 640 Gregor, L. and Gruber, N.: OceanSODA-ETHZ: A Global Gridded Data Set of the Surface Ocean Carbonate System for Seasonal to Decadal Studies of Ocean Acidification, *Earth System Science Data*, 13, 777–808, <https://doi.org/10.5194/essd-13-777-2021>, 2021.
- Grosell, M.: Intestinal Anion Exchange in Marine Teleosts Is Involved in Osmoregulation and Contributes to the Oceanic Inorganic Carbon Cycle, *Acta Physiol (Oxf)*, 202, 421–434, <https://doi.org/10.1111/j.1748-1716.2010.02241.x>, 2011.
- Hashim, M. S., Conte, M. H., Salter, M. A., Pedrosa-Pamies, R., Weber, J. C., Hayden, M. G., Wilson, R. W., Perry, C. T., Crowley, S. F., Dennis, P. F., Bish, D., and Subhas, A. V.: Fish Carbonates in the North Atlantic and Their Potential Role in the Carbon Cycle, *Global 645 Biogeochemical Cycles*, 39, e2024GB008 387, <https://doi.org/10.1029/2024GB008387>, 2025.
- Humphreys, M. P. and Schiller, A. J.: Pytzer: The Pitzer Model for Chemical Activities in Aqueous Solutions in Python (Beta), Zenodo, <https://doi.org/10.5281/zenodo.14353294>, 2024.
- Humphreys, M. P., Cala, B. A., Schiller, A. J., Sandborn, D., Gregor, L., Pierrot, D., van Heuven, S. M. A. C., Lewis, E. R., and Wallace, D. W. R.: PyCO2SYS: Marine Carbonate System Calculations in Python, Zenodo, <https://doi.org/10.5281/zenodo.16738120>, 2025.



- 650 650 Ingle, S.: Solubility of Calcite in the Ocean, *Marine Chemistry*, 3, 301–319, [https://doi.org/10.1016/0304-4203\(75\)90010-9](https://doi.org/10.1016/0304-4203(75)90010-9), 1975.
Koskamp, J. A., Ruiz Hernandez, S. E. R., Leeuw, N. H. D., and Wolthers, M.: First Steps towards Understanding the Non-Linear Impact of Mg on Calcite Solubility: A Molecular Dynamics Study, *Minerals*, 11, 407, <https://doi.org/10.3390/min11040407>, 2021.
Kwon, E. Y., Dunne, J. P., and Lee, K.: Biological Export Production Controls Upper Ocean Calcium Carbonate Dissolution and CO₂ Buffer Capacity, *Science Advances*, 10, eadl0779, <https://doi.org/10.1126/sciadv.adl0779>, 2024.
- 655 655 Lafon, G. M.: Equilibrium Criteria for Two-Component Solids Reacting with Fixed Composition in an Aqueous Phase; Example, the Magnesian Calcites; Discussion, *American Journal of Science*, 278, 1455–1468, 1978.
Lauvset, S. K., Lange, N., Tanhua, T., Bittig, H. C., Olsen, A., Kozyr, A., Álvarez, M., Azetsu-Scott, K., Becker, S., Brown, P. J., Carter, B. R., Cotrim da Cunha, L., Feely, R. A., Hoppema, M., Humphreys, M. P., Ishii, M., Jeansson, E., Jones, S. D., Lo Monaco, C., Murata, A., Müller, J. D., Pérez, F. F., Schirnick, C., Steinfeldt, R., Suzuki, T., Tilbrook, B., Ulfsbo, A., Velo, A., Woosley, R. J., and Key, R. M.: Global Ocean Data Analysis Project Version 2.2023 (GLODAPv2.2023) (NCEI Accession 0283442), <https://doi.org/10.25921/ZYRQ-HT66>, 2023.
- 660 660 Lauvset, S. K., Lange, N., Tanhua, T., Bittig, H. C., Olsen, A., Kozyr, A., Álvarez, M., Azetsu-Scott, K., Brown, P. J., Carter, B. R., Cotrim Da Cunha, L., Hoppema, M., Humphreys, M. P., Ishii, M., Jeansson, E., Murata, A., Müller, J. D., Pérez, F. F., Schirnick, C., Steinfeldt, R., Suzuki, T., Ulfsbo, A., Velo, A., Woosley, R. J., and Key, R. M.: The Annual Update GLODAPv2.2023: The Global Interior Ocean Biogeochemical Data Product, *Earth Syst. Sci. Data*, 16, 2047–2072, <https://doi.org/10.5194/essd-16-2047-2024>, 2024.
- 665 665 Liang, H., Lunstrum, A. M., Dong, S., Berelson, W. M., and John, S. G.: Constraining CaCO₃ Export and Dissolution With an Ocean Alkalinity Inverse Model, *Global Biogeochemical Cycles*, 37, e2022GB007535, <https://doi.org/10.1029/2022GB007535>, 2023.
Lueker, T. J., Dickson, A. G., and Keeling, C. D.: Ocean pCO₂ Calculated from Dissolved Inorganic Carbon, Alkalinity, and Equations for K1 and K2: Validation Based on Laboratory Measurements of CO₂ in Gas and Seawater at Equilibrium, *Marine Chemistry*, 70, 105–119, [https://doi.org/10.1016/S0304-4203\(00\)00022-0](https://doi.org/10.1016/S0304-4203(00)00022-0), 2000.
- 670 670 Mackenzie, F., Bischoff, W., Bishop, F., Loijens, M., Schoonmaker, J., and Wollast, R.: Chapter 4. Magnesian Calcites: Low-Temperature Occurrence, Solubility and Solid-Solution Behavior, in: *Carbonates: Mineralogy and Chemistry*, edited by Reeder, R. J., pp. 97–144, De Gruyter, ISBN 978-1-5015-0813-4, <https://doi.org/10.1515/9781501508134-008>, 1983.
Millero, F. J.: The Thermodynamics of the Carbonate System in Seawater, *Geochimica et Cosmochimica Acta*, 43, 1651–1661, [https://doi.org/10.1016/0016-7037\(79\)90184-4](https://doi.org/10.1016/0016-7037(79)90184-4), 1979.
- 675 675 Millero, F. J., Feistel, R., Wright, D. G., and McDougall, T. J.: The Composition of Standard Seawater and the Definition of the Reference-Composition Salinity Scale, *Deep Sea Research Part I: Oceanographic Research Papers*, 55, 50–72, <https://doi.org/10.1016/j.dsr.2007.10.001>, 2008.
Milliman, J. D.: Dissolution of Calcium Carbonate in the Sargasso Sea (Northwest Atlantic), in: *The Fate of Fossil Fuel CO₂ in the Oceans*, edited by Andersen, N. R. and Malahoff, A., pp. 641–653, Plenum Press, <https://doi.org/10.1007/978-1-4899-5016-1>, 1977.
- 680 680 Milliman, J. D., Troy, P. J., Balch, W. M., Adams, A. K., Li, Y. H., and Mackenzie, F. T.: Biologically Mediated Dissolution of Calcium Carbonate above the Chemical Lysocline?, *Deep Sea Research Part I: Oceanographic Research Papers*, 46, 1653–1669, [https://doi.org/10.1016/S0967-0637\(99\)00034-5](https://doi.org/10.1016/S0967-0637(99)00034-5), 1999.
Moberly, R.: Composition of Magnesian Calcites of Algae and Pelecypods by Electron Microprobe Analysis, *Sedimentology*, 11, 61–82, <https://doi.org/10.1111/j.1365-3091.1968.tb00841.x>, 1968.
Morse, J. W. and Mackenzie, F. T.: *Geochemistry of Sedimentary Carbonates*, Elsevier, ISBN 978-0-08-086962-9, 1990.



- Morse, J. W., Andersson, A. J., and Mackenzie, F. T.: Initial Responses of Carbonate-Rich Shelf Sediments to Rising Atmospheric pCO₂ and “Ocean Acidification”: Role of High Mg-calcites, *Geochimica et Cosmochimica Acta*, 70, 5814–5830, <https://doi.org/10.1016/j.gca.2006.08.017>, 2006.
- 690 Mucci, A.: The Solubility of Calcite and Aragonite in Seawater at Various Salinities, Temperatures, and One Atmosphere Total Pressure, *American Journal of Science*, 283, 780–799, <https://doi.org/10.2475/ajs.283.7.780>, 1983.
- Mucci, A.: Influence of Temperature on the Composition of Magnesian Calcite Overgrowths Precipitated from Seawater, *Geochimica et Cosmochimica Acta*, 51, 1977–1984, [https://doi.org/10.1016/0016-7037\(87\)90186-4](https://doi.org/10.1016/0016-7037(87)90186-4), 1987.
- 695 Mucci, A. and Morse, J.: The Solubility of Calcite in Seawater Solutions of Various Magnesium Concentration, It = 0.697 m at 25 °C and One Atmosphere Total Pressure, *Geochim. Cosmochim. Acta*, 48, 815–822, [https://doi.org/10.1016/0016-7037\(84\)90103-0](https://doi.org/10.1016/0016-7037(84)90103-0), 1984.
- Naviaux, J. D., Subhas, A. V., Dong, S., Rollins, N. E., Liu, X., Byrne, R. H., Berelson, W. M., and Adkins, J. F.: Calcite Dissolution Rates in Seawater: Lab vs. *in-Situ* Measurements and Inhibition by Organic Matter, *Marine Chemistry*, 215, 103 684, <https://doi.org/10.1016/j.marchem.2019.103684>, 2019.
- Oehlert, A. M., Garza, J., Nixon, S., Frank, L., Folkerts, E. J., Stieglitz, J. D., Lu, C., Heuer, R. M., Benetti, D. D., del Campo, J., Gomez, 700 F. A., and Grosell, M.: Implications of Dietary Carbon Incorporation in Fish Carbonates for the Global Carbon Cycle, *Science of The Total Environment*, 916, 169 895, <https://doi.org/10.1016/j.scitotenv.2024.169895>, 2024a.
- Oehlert, A. M., Walls, S., Arista, K., Garza, J., Folkerts, E. J., Vitek, B. E., Tale Masoule, S., Pollier, C. G. L., Duchâtelier, G., Stieglitz, J. D., Benetti, D. D., Heuer, R. M., Ghahremaninezhad, A., and Grosell, M.: Organic Coatings Reduce Dissolution Rate by an Order of Magnitude for Carbonate Minerals Produced by Marine Fish, *Global Biogeochemical Cycles*, 38, e2024GB008 176, 705 <https://doi.org/10.1029/2024GB008176>, 2024b.
- Orr, J. C., Fabry, V. J., Aumont, O., Bopp, L., Doney, S. C., Feely, R. A., Gnanadesikan, A., Gruber, N., Ishida, A., Joos, F., Key, R. M., Lindsay, K., Maier-Reimer, E., Matear, R., Monfray, P., Mouchet, A., Najjar, R. G., Plattner, G.-K., Rodgers, K. B., Sabine, C. L., Sarmiento, J. L., Schlitzer, R., Slater, R. D., Totterdell, I. J., Weirig, M.-F., Yamanaka, Y., and Yool, A.: Anthropogenic Ocean Acidification over the Twenty-First Century and Its Impact on Calcifying Organisms, *Nature*, 437, 681–686, <https://doi.org/10.1038/nature04095>, 2005.
- 710 Paquette, J. and Reeder, R. J.: Single-Crystal X-ray Structure Refinements of Two Biogenic Magnesian Calcite Crystals, *American Mineralogist*, 75, 1151–1158, 1990.
- Pedrosa-Pamies, R., Conte, M. H., Weber, J. C., and Andersson, A. J.: Hurricane-Driven Transport of Bermuda Reef Carbonate Platform Sediments to the Deep Ocean, *Journal of Geophysical Research: Oceans*, 130, e2023JC020 500, <https://doi.org/10.1029/2023JC020500>, 2025.
- 715 Perry, C. T., Salter, M. A., Harborne, A. R., Crowley, S. F., Jelks, H. L., and Wilson, R. W.: Fish as Major Carbonate Mud Producers and Missing Components of the Tropical Carbonate Factory, *Proc Natl Acad Sci U S A*, 108, 3865–3869, <https://doi.org/10.1073/pnas.1015895108>, 2011.
- Plummer, L. N. and Busenberg, E.: The Solubilities of Calcite, Aragonite and Vaterite in CO₂-H₂O Solutions between 0 and 90°C, and an Evaluation of the Aqueous Model for the System CaCO₃-CO₂-H₂O, *Geochimica et Cosmochimica Acta*, 46, 1011–1040, 720 [https://doi.org/10.1016/0016-7037\(82\)90056-4](https://doi.org/10.1016/0016-7037(82)90056-4), 1982.
- Plummer, L. N. and Mackenzie, F. T.: Predicting Mineral Solubility from Rate Data; Application to the Dissolution of Magnesian Calcites, *American Journal of Science*, 274, 61–83, <https://doi.org/10.2475/ajs.274.1.61>, 1974.
- Reed, J. J.: The NBS Tables of Chemical Thermodynamic Properties: Selected Values for Inorganic and C1 and C2 Organic Substances in SI Units, <https://doi.org/10.18434/M32124>, 2020.



- 725 Riley, J. P. and Tongudai, M.: The Major Cation/Chlorinity Ratios in Sea Water, *Chemical Geology*, 2, 263–269, [https://doi.org/10.1016/0009-2541\(67\)90026-5](https://doi.org/10.1016/0009-2541(67)90026-5), 1967.
- Robie, R. A. and Bethke, P. M.: Molar Volumes and Densities of Minerals, *Tech. Rep. 822*, U.S. Geological Survey, <https://doi.org/10.3133/70159012>, 1962.
- Robie, R. A. and Hemingway, B. S.: Thermodynamic Properties of Minerals and Related Substances at 298.15 K and 1 Bar (10⁵ Pascals) Pressure and at Higher Temperatures, *Tech. Rep. 2131*, U.S. Geological Survey, Information Services, <https://doi.org/10.3133/b2131>, 1995.
- 730 Salter, M. A., Perry, C. T., and Wilson, R. W.: Production of Mud-Grade Carbonates by Marine Fish: Crystalline Products and Their Sedimentary Significance, *Sedimentology*, 59, 2172–2198, <https://doi.org/10.1111/j.1365-3091.2012.01339.x>, 2012.
- Sarmiento, J. L. and Gruber, N.: *Ocean Biogeochemical Dynamics*, Princeton University Press, ISBN 978-1-4008-4907-9, <https://doi.org/10.1515/9781400849079>, 2013.
- 735 Subhas, A. V., Dong, S., Naviaux, J. D., Rollins, N. E., Ziveri, P., Gray, W., Rae, J. W. B., Liu, X., Byrne, R. H., Chen, S., Moore, C., Martell-Bonet, L., Steiner, Z., Antler, G., Hu, H., Lunstrum, A., Hou, Y., Kemnitz, N., Stutsman, J., Pallacks, S., Dugenne, M., Quay, P. D., Berelson, W. M., and Adkins, J. F.: Shallow Calcium Carbonate Cycling in the North Pacific Ocean, *Global Biogeochemical Cycles*, 36, e2022GB007388, <https://doi.org/10.1029/2022GB007388>, 2022.
- 740 Sulpis, O., Jeansson, E., Dinauer, A., Lauvset, S. K., and Middelburg, J. J.: Calcium Carbonate Dissolution Patterns in the Ocean, *Nat. Geosci.*, 14, 423–428, <https://doi.org/10.1038/s41561-021-00743-y>, 2021.
- Sulpis, O., Agrawal, P., Wolthers, M., Munhoven, G., Walker, M., and Middelburg, J. J.: Aragonite Dissolution Protects Calcite at the Seafloor, *Nat Commun*, 13, 1104, <https://doi.org/10.1038/s41467-022-28711-z>, 2022.
- 745 Thorstenson, D. C. and Plummer, N.: Equilibrium Criteria for Two-Component Solids Reacting with Fixed Composition in an Aqueous Phase; Example, the Magnesian Calcites, *American Journal of Science*, 277, 1203–1223, <https://doi.org/10.2475/AJS.277.9.1203>, 1977.
- Uppström, L. R.: The Boron/Chlorinity Ratio of Deep-Sea Water from the Pacific Ocean, *Deep Sea Research and Oceanographic Abstracts*, 21, 161–162, [https://doi.org/10.1016/0011-7471\(74\)90074-6](https://doi.org/10.1016/0011-7471(74)90074-6), 1974.
- Virtanen, P., Gommers, R., Oliphant, T. E., Haberland, M., Reddy, T., Cournapeau, D., Burovski, E., Peterson, P., Weckesser, W., Bright, J., van der Walt, S. J., Brett, M., Wilson, J., Millman, K. J., Mayorov, N., Nelson, A. R. J., Jones, E., Kern, R., Larson, E., Carey, C. J., Polat, 750 Í., Feng, Y., Moore, E. W., VanderPlas, J., Laxalde, D., Perktold, J., Cimrman, R., Henriksen, I., Quijano, E. A., Harris, C. R., Archibald, A. M., Ribeiro, A. H., Pedregosa, F., and van Mulbregt, P.: SciPy 1.0: Fundamental Algorithms for Scientific Computing in Python, *Nat Methods*, 17, 261–272, <https://doi.org/10.1038/s41592-019-0686-2>, 2020.
- Walsh, P. J., Blackwelder, P., Gill, K. A., Danulat, E., and Mommsen, T. P.: Carbonate Deposits in Marine Fish Intestines: A New Source of Biomineralization, *Limnology and Oceanography*, 36, 1227–1232, <https://doi.org/10.4319/lo.1991.36.6.1227>, 1991.
- 755 Walter, L. M. and Morse, J. W.: Magnesian Calcite Stabilities: A Reevaluation, *Geochimica et Cosmochimica Acta*, 48, 1059–1069, [https://doi.org/10.1016/0016-7037\(84\)90196-0](https://doi.org/10.1016/0016-7037(84)90196-0), 1984.
- White, M. M., Waller, J. D., Lubelczyk, L. C., Drapeau, D. T., Bowler, B. C., Balch, W. M., and Fields, D. M.: Coccolith Dissolution within Copepod Guts Affects Fecal Pellet Density and Sinking Rate, *Sci Rep*, 8, 9758, <https://doi.org/10.1038/s41598-018-28073-x>, 2018.
- Wilson, R. W., Millero, F. J., Taylor, J. R., Walsh, P. J., Christensen, V., Jennings, S., and Grosell, M.: Contribution of Fish to the Marine 760 Inorganic Carbon Cycle, *Science*, 323, 359–362, <https://doi.org/10.1126/science.1157972>, 2009.
- Woosley, R. J., Millero, F. J., and Grosell, M.: The Solubility of Fish-Produced High Magnesium Calcite in Seawater, *Journal of Geophysical Research: Oceans*, 117, <https://doi.org/10.1029/2011JC007599>, 2012.